Journal of Computational Physics 395 (2019) 382–409

Contents lists available at ScienceDirect

Journal of Computational Physics

www.elsevier.com/locate/jcp

A second order fully-discrete linear energy stable scheme for a binary compressible viscous fluid model

Xueping Zhao [a], Qi Wang [b,c,*]

[a] Max Planck Institute for the Physics of Complex Systems, Nöthnitzer Str. 38, 01187 Dresden, Germany
[b] Department of Mathematics, University of South Carolina, Columbia, SC, 29208, USA
[c] Beijing Computational Science Research Center, Beijing 100193, China

ARTICLE INFO

Article history:
Received 8 September 2018
Received in revised form 26 April 2019
Accepted 11 June 2019
Available online 13 June 2019

Keywords:
Binary compressible fluid flows
Energy quadratization
Energy stable schemes
Finite difference methods

ABSTRACT

We present a linear, second order fully discrete numerical scheme on a staggered grid for a thermodynamically consistent hydrodynamic phase field model of binary compressible fluid flows, derived from the generalized Onsager Principle. The hydrodynamic model possesses not only the variational structure in its constitutive equation, but also warrants the mass, linear momentum conservation as well as energy dissipation. We first reformulate the model using the energy quadratization method into an equivalent form and then discretize the reformulated model to obtain a semidiscrete partial differential equation system using the Crank-Nicolson method in time. The semi-discrete numerical scheme preserves the mass conservation and energy dissipation law in time. Then, we discretize the semi-discrete PDE system on a staggered grid in space to arrive at a fully discrete scheme using 2nd order finite difference methods, which respects a discrete energy dissipation law. We prove the unique solvability of the linear system resulting from the fully discrete scheme. Mesh refinements and numerical examples on phase separation due to spinodal decomposition in binary polymeric fluids and interface evolution in the gas-liquid mixture are presented to show the convergence property and the usefulness of the new scheme in applications, respectively.

1. Introduction

Material systems comprising of multi-components, some of which are compressible while others are incompressible, are ubiquitous in nature and industrial applications. For example, in growing tissues, cell proliferation makes the material volume changes so that it can not be described as incompressible [25]. Another example of the mixture of compressible fluids is the binary fluid flows of non-hydrocarbon (e.g. CO_2) and hydrocarbons encountered in the enhanced oil recovery (EOR) process. Since gas (e.g. CO_2) injection offers considerable potential benefits to oil recovery attracting the most new market interest since 1972, properties (viscosity, density et al.) of multi-component compressible mixtures of nonhydrocarbon and hydrocarbons have been studied by a number of investigators [12,31,40].

Phase field methods have been used successfully to formulate models for fluid mixtures in many applications ranging from biological sciences [43,44,51,67], including cell biology [27,38,61,68,69], biofilms [56–58], cell adhesion and motility [6,33,37–39], cell membrane [2,3,18,49,52], tumor growth [51]), to materials science [5,7,14], fluid dynamics [34,35,48], and

* Corresponding author.
E-mail address: qwang@math.sc.edu (Q. Wang).

https://doi.org/10.1016/j.jcp.2019.06.030
0021-9991/

image processing [4,30,65] et al. The most widely studied phase field model for binary fluid mixtures is the one for fluid mixtures of two incompressible fluids of identical densities [1,26,32]. While modeling binary fluid mixtures using phase field models, one commonly uses a phase variable ϕ, either a volume fraction or a mass fraction of a fluid component, to distinguish between distinct material phases. For instance $\phi = 1$ indicates one fluid phase while $\phi = 0$ denotes another fluid phase in the immiscible, binary fluid mixture. For immiscible mixtures, the interfacial region between different phases is described by $0 < \phi < 1$. A transport equation for phase variable ϕ along with conservation equations of mass and momentum and the constitutive equation constitute the governing system of equations for the binary incompressible fluid mixture.

In the compressible fluid flow, we use the mass density ρ_i or molar density n_i in place of volume fraction ϕ_i $(i = 1, 2)$, to represent the distribution of each compressible component in the fluid mixture. The material compressibility comes from two sources. One is the material compressibility itself and the other is the mass-generating source. In general, the transport equation for the mass density of each component is given by

$$\frac{\partial \rho_i}{\partial t} + \nabla \cdot (\rho_i \mathbf{v_i}) = j_i, \qquad i = 1, \cdots, N, \tag{1.1}$$

or the transport equation for the molar density is given by

$$\frac{\partial n_i}{\partial t} + \nabla \cdot (n_i \mathbf{v_i}) = j_i, \qquad i = 1, \cdots, N, \tag{1.2}$$

where $\mathbf{v}_i$ is the velocity of the ith component, j_i is the mass source or molar source of the ith component. The transport equations for the mass or molar densities, constitutive equation for the stress, the conservation laws of mass and momentum constitute the governing equations of the hydrodynamic phase field models of the compressible fluid mixtures.

Distinguishing properties of the compressible hydrodynamic phase field models include that the density of each compressible material component is a variable, the mass average velocity of the fluid flow is most likely not solenoidal, and the pressure is determined by the equation of state or the free energy of the mixture system (at least in the isothermal case). In [35], Truskinovsky and Lowengrub derived the Navier–Stokes–Cahn–Hilliard (NSCH) system for a binary mixture of two incompressible fluid flows with unmatched densities in the fluid components, in which the mass concentration of one fluid component in the binary fluid flow is used as the phase variable. They named the hydrodynamic phase field model the quasi-incompressible model. They also discussed the compressible model of binary fluids briefly. Guo and Lin gave a systematic derivation of a nonisothermal hydrodynamic model for binary compressible fluids in [24]. In [28,29], Sun et al. propose a general diffuse interface model with a given equation of state (e.g. Peng-Robinson equation of state) to describe the multi-component fluid flow based on the principles of the NVT-based framework. In [64], we systematically derived a thermodynamically consistent hydrodynamic phase field model for multi-component compressible fluid mixtures through a variational approach coupled with the generalized Onsager Principle [55] and discussed various means to arrive at the quasi-incompressible limit and the fully incompressible limit. In this paper, we develop an unconditionally energy stable numerical algorithm to solve the thermodynamically consistent, hydrodynamic phase field model for multi-component compressible fluid flows.

The hydrodynamic phase field model for compressible fluid flows is nonlinear, exemplified in its free energy, mobility coefficients and in the transport equations. High order approximation, unconditional energy stability as well as computational efficiency are desired properties to attain in developing its numerical approximation. To preserve the energy dissipation property in numerical approximations, several time-marching approaches have been developed in the past: convex splitting method [8,10,15,16], stabilization method [46,66], and energy quadratization (EQ, including SAV) approach [21,60,63]. The convex splitting method has been used to obtain a series of first order energy stable schemes for various PDE models exhibiting energy dissipation properties. However, the convex-splitting scheme is usually nonlinear and therefore can be expensive to solve from time to time. On the other hand, even though it is possible to construct a second order convex splitting scheme in some cases, it was usually done on a case by case basis and a general formulation is not yet available. The stabilization method is another method for obtaining energy stable numerical approximations, which is equivalent to a convex splitting method in some cases. By adding a linear, stabilizing operator in the order of the truncation error, one can obtain an energy stable algorithm. In general, a second order stabilizing scheme can be derived to preserve energy decay at the discrete level but not the energy dissipation rate. The energy quadratization(EQ), also known as the invariant energy quadratization (IEQ), method was proposed recently [22,53,54] and extended to various gradient flows and hydrodynamic phase field models [21,60,63]. By introducing intermediate variables, one can rewrite the nonlinear free energy functional in an arbitrary form into a quadratic form and recast the governing system of equations into an equivalent form. For the transformed system with a quadratic free energy, a linear second order or even higher order numerical scheme can be constructed [19,59,62].

Recently, Sun et al. [28,29] used the convex splitting approach and the scalar auxiliary variable method [47], respectively, to solve a binary compressible hydrodynamic phase field model. They obtained some first order semi-discrete schemes. In this paper, we focus on developing a linear, second order, fully discrete numerical scheme for the hydrodynamic phase field model for binary compressible fluid flows based on the energy quadratization strategy. We will show that this scheme is second order, unconditionally energy stable and the linear system resulting from the numerical scheme is uniquely solvable. At each time step, the linear algebraic system is solved using a pre-conditioner. Two examples on phase separation dynamics in viscous polymeric blends and interface evolution in gas-liquid mixtures are presented to show the usefulness of the new schemes in some practical applications.

The paper is organized as follows. In §2, we briefly recall the derivation of the compressible hydrodynamic phase field model. Its non-dimensionalization is given in §3. In §4, we reformulate the model using the energy quadratization method. The fully discrete numerical scheme, where we use second order finite difference in space and "linearized" Crank-Nicolson method in time, is given in §5. The unique solvability of the linear system resulting from the scheme and preservation of the energy dissipation rate are proved as well. In §6, we show several numerical experiments that validate the accuracy, stability and efficiency of the numerical scheme. We give concluding remarks in §7.

2. Thermodynamically consistent hydrodynamic phase field models for binary compressible viscous fluid flows

A general thermodynamically consistent hydrodynamic phase field model for fluid flows of n viscous fluid components has been derived in [64]. Here, we briefly recall the basic ingredients in the binary fluid model and discuss its energy dissipation property. We consider flows of binary compressible viscous fluids with densities ρ_1 and ρ_2, respectively. The mass conservation equation for each fluid component is respectively given by

$$\frac{\partial \rho_i}{\partial t} + \nabla \cdot (\rho_i \mathbf{v}_i) = 0, \quad i = 1, 2, \tag{2.1}$$

where $\mathbf{v}_i$ is the velocity of the ith fluid component, $i = 1, 2$. We define the total mass of the fluid mixture as $\rho = \rho_1 + \rho_2$ and the mass average velocity as $\mathbf{v} = \frac{1}{\rho}(\rho_1 \mathbf{v}_1 + \rho_2 \mathbf{v}_2)$. Then, the mass conservation equation for the total mass density ρ is given by

$$\frac{\partial \rho}{\partial t} + \nabla \cdot (\rho \mathbf{v}) = 0. \tag{2.2}$$

Using the mass average velocity, we rewrite the mass transport equation as follows

$$\frac{\partial \rho_i}{\partial t} + \nabla \cdot (\rho_i \mathbf{v}) = j_i = \nabla \cdot \mathbf{J}_i, \quad i = 1, 2, \tag{2.3}$$

where $\mathbf{J}_i = \rho_i(\mathbf{v} - \mathbf{v}_i)$ is the excessive mass flux of fluid $i = 1, 2$, and $j_1 + j_2 = 0$ according to the total mass conservation law. The linear momentum conservation law of the fluid mixture is given by

$$\frac{\partial (\rho \mathbf{v})}{\partial t} + \nabla \cdot (\rho \mathbf{v}\mathbf{v}) = \nabla \cdot \sigma + \mathbf{b} \tag{2.4}$$

derived from the momentum conservation for each fluid component, where $\mathbf{b}$ is the body force, σ is the total stress tensor, $\sigma = \sigma^s + \sigma^e$, σ^s is the symmetric viscous stress tensor, and σ^e is the Ericksen stress tensor. Both $\mathbf{J}_i$, $i = 1, 2$ and σ^s would be determined by constitutive relations later.

For the compressible fluid mixture, we assume the free energy of the system is given by

$$F = \int_V f(\rho_1, \rho_2, \nabla \rho_1, \nabla \rho_2) d\mathbf{x}, \tag{2.5}$$

where f is the free energy density function and V is the domain in which the fluid mixture occupies. The total energy of the fluid system is given by the sum of the kinetic energy and the free energy:

$$E = \int_V [\tfrac{1}{2}\rho ||\mathbf{v}||^2 + f] d\mathbf{x}. \tag{2.6}$$

Considering the conservation laws of mass and linear momentum, we calculate the energy dissipation rate as follows

$$\begin{aligned} \frac{dE}{dt} &= \int_V [-\sigma^s : \mathbf{D} + (\mathbf{b} + \nabla \cdot \sigma^e + \rho_1 \nabla \mu_1 + \rho_2 \nabla \mu_2) \cdot \mathbf{v} + \mu_1 j_1 + \mu_2 j_2] d\mathbf{x} \\ &+ \int_{\partial V} [(\sigma^s \cdot \mathbf{v}) \cdot \mathbf{n} - \tfrac{1}{2}(\rho \mathbf{v} \|\mathbf{v}\|^2) \cdot \mathbf{n} + (-\mu_1 \rho_1 \mathbf{v} - \mu_2 \rho_2 \mathbf{v} + \tfrac{\partial f}{\partial (\nabla \rho_1)} \tfrac{\partial \rho_1}{\partial t} + \tfrac{\partial f}{\partial (\nabla \rho_2)} \tfrac{\partial \rho_2}{\partial t}) \cdot \mathbf{n}] dS, \end{aligned} \tag{2.7}$$

where $\mathbf{D} = \frac{1}{2}(\nabla \mathbf{v} + \nabla \mathbf{v}^T)$ is the rate of strain tensor, $\mathbf{n}$ is the unit external normal of the domain boundary ∂V, $\mu_1 = \frac{\partial f}{\partial \rho_1} - \nabla \cdot \frac{\partial f}{\partial \nabla \rho_1}$, $\mu_2 = \frac{\partial f}{\partial \rho_2} - \nabla \cdot \frac{\partial f}{\partial \nabla \rho_2}$ are the chemical potentials with respect to ρ_1 and ρ_2, respectively. We identify the Erickson stress by the equation

$$\nabla \cdot \sigma^e = -\rho_1 \nabla \mu_1 - \rho_2 \nabla \mu_2. \tag{2.8}$$

The energy dissipation rate reduces to

$$\begin{aligned} \frac{dE}{dt} &= \int_V [\mathbf{b} \cdot \mathbf{v} - \sigma^s : \mathbf{D} + \mu_1 j_1 + \mu_2 j_2] d\mathbf{x} + \int_{\partial V} [(\sigma^s \cdot \mathbf{v}) \cdot \mathbf{n} - \tfrac{1}{2}(\rho \mathbf{v} \|\mathbf{v}\|^2) \cdot \mathbf{n} \\ &+ (-\mu_1 \rho_1 \mathbf{v} - \mu_2 \rho_2 \mathbf{v} + \tfrac{\partial f}{\partial (\nabla \rho_1)} \tfrac{\partial \rho_1}{\partial t} + \tfrac{\partial f}{\partial (\nabla \rho_2)} \tfrac{\partial \rho_2}{\partial t}) \cdot \mathbf{n}] dS. \end{aligned} \tag{2.9}$$

In the bulk integral, we propose the following constitutive relations following the generalized Onsager principle

$$\begin{aligned} \sigma^s &= 2\eta \mathbf{D} + \overline{\eta} tr(\mathbf{D}) \mathbf{I}, \\ j_i &= -\textstyle\sum_{k=1}^{2} \nabla \cdot M_{ik} \cdot \nabla \mu_k, i = 1, 2, \end{aligned} \tag{2.10}$$

where η, $\bar{\eta}$ are the shear and volumetric viscosity respectively, and $\mathcal{M} = (M_{ik})_{2\times 2} \geq 0$ is the symmetric mobility matrix. Since $\sum_{i=1}^{2} j_i = 0$ according to the mass conservation law, this imposes a constraint $\mathcal{M}\cdot\mathbf{1} = \mathbf{0}$, where $\mathbf{1}^T = (1,1)$. Examining the surface integral, we notice that if we assume the following conditions

$$\mathbf{v}|_{\partial V} = 0, \qquad \mathbf{n}\cdot\nabla\mu_i|_{\partial V} = 0, \qquad \mathbf{n}\cdot\frac{\partial f}{\partial(\nabla\rho_i)}|_{\partial V} = 0, (\text{ or } \rho_i = \rho_i(\mathbf{x})), \quad i = 1,2, \tag{2.11}$$

on the boundary, the surface integral vanishes in the energy dissipation function. So, at the absence of the body force $\mathbf{b} = \mathbf{0}$, the total energy dissipation rate reduces to

$$\frac{dE}{dt} = -\int_V [2\eta\mathbf{D}:\mathbf{D} + \overline{\eta}tr(\mathbf{D})^2 + (\nabla\mu_1, \nabla\mu_2)\cdot\mathcal{M}\cdot(\nabla\mu_1, \nabla\mu_2)^T]d\mathbf{x} \leq 0, \tag{2.12}$$

provided $\eta, \overline{\eta} \geq 0, \mathcal{M} \geq 0$.

Remark 2.1. If we choose the boundary conditions as follows

$$\mathbf{v}\cdot\mathbf{n} = 0, \qquad \sigma_s\cdot\mathbf{n} = -\beta(\mathbf{I}-\mathbf{nn})\cdot\mathbf{v}, \qquad \mathbf{n}\cdot\frac{\partial f}{\partial(\nabla\rho_1)} = -\gamma_1\frac{\partial\rho_1}{\partial t}, \qquad \mathbf{n}\cdot\frac{\partial f}{\partial(\nabla\rho_2)} = -\gamma_2\frac{\partial\rho_2}{\partial t}, \tag{2.13}$$

where $\beta, \gamma_1, \gamma_2 \geq 0$, the energy dissipation rate is given by

$$\begin{aligned}\frac{dE}{dt} = &-\int_V [2\eta\mathbf{D}:\mathbf{D} + \overline{\eta}tr(\mathbf{D})^2 + (\nabla\mu_1, \nabla\mu_2)\cdot\mathcal{M}\cdot(\nabla\mu_1, \nabla\mu_2)^T]d\mathbf{x}\\ &-\int_{\partial V}[\beta(\mathbf{I}-\mathbf{nn})\|\mathbf{v}\|^2 + \gamma_1(\frac{\partial\rho_1}{\partial t})^2 + \gamma_2(\frac{\partial\rho_2}{\partial t})^2]ds.\end{aligned} \tag{2.14}$$

These boundary conditions allow fluid flows slip at the boundary and mass fluxes to move through the boundary, which leads to additional energy dissipation at the surface. We will not pursue these boundary conditions in this study, which worthy of a complete study of its own.

We summarize the governing system of equations of the compressible binary fluid system as follows:

$$\begin{cases}\frac{\partial\rho_1}{\partial t} + \nabla\cdot(\rho_1\mathbf{v}) = \nabla\cdot M_{11}\cdot\nabla\mu_1 + \nabla\cdot M_{12}\cdot\nabla\mu_2,\\ \frac{\partial\rho_2}{\partial t} + \nabla\cdot(\rho_2\mathbf{v}) = \nabla\cdot M_{21}\cdot\nabla\mu_1 + \nabla\cdot M_{22}\cdot\nabla\mu_2,\\ \frac{\partial(\rho\mathbf{v})}{\partial t} + \nabla\cdot(\rho\mathbf{vv}) = 2\nabla\cdot(\eta\mathbf{D}) + \nabla(\overline{\eta}\nabla\cdot\mathbf{v}) - \rho_1\nabla\mu_1 - \rho_2\nabla\mu_2,\end{cases} \tag{2.15}$$

where $\sum_{i,k=1}^{2}\nabla\cdot M_{ik}\cdot\nabla\mu_k = 0$. One particular mobility matrix satisfying the constraint consists of the entries $M_1 = M_{11} = -M_{12} = -M_{21} = M_{22}$. In this case, the governing equations reduce to

$$\begin{cases}\frac{\partial\rho_1}{\partial t} + \nabla\cdot(\rho_1\mathbf{v}) = \nabla\cdot M_1\cdot\nabla(\mu_1-\mu_2),\\ \frac{\partial\rho_2}{\partial t} + \nabla\cdot(\rho_2\mathbf{v}) = -\nabla\cdot M_1\cdot\nabla(\mu_1-\mu_2),\\ \frac{\partial(\rho\mathbf{v})}{\partial t} + \nabla\cdot(\rho\mathbf{vv}) = 2\nabla\cdot(\eta\mathbf{D}) + \nabla(\overline{\eta}\nabla\cdot\mathbf{v}) - \rho_1\nabla\mu_1 - \rho_2\nabla\mu_2.\end{cases} \tag{2.16}$$

For the viscosity coefficients, we denote η_1, η_2 as the shear viscosities of the fluid component 1 and 2 respectively, and $\overline{\eta}_1, \overline{\eta}_2$ as the volumetric viscosities of the two components. $\eta, \overline{\eta}$ are chosen as the mass average viscosities of the two components:

$$\eta = \frac{1}{\rho}[\rho_1\eta_1 + \rho_2\eta_2], \qquad \overline{\eta} = \frac{1}{\rho}[\rho_1\overline{\eta}_1 + \rho_2\overline{\eta}_2]. \tag{2.17}$$

In this study, we focus on the free energy density function f in the following form

$$f(\rho_1, \rho_2, \nabla\rho_1, \nabla\rho_2, T) = h(\rho_1, \rho_2, T) + \frac{1}{2}[\kappa_{\rho_1\rho_1}(\nabla\rho_1)^2 + 2\kappa_{\rho_1\rho_2}(\nabla\rho_1, \nabla\rho_2) + \kappa_{\rho_2\rho_2}(\nabla\rho_2)^2], \tag{2.18}$$

where $h(\rho_1, \rho_2, T)$ is the homogeneous or the bulk free energy density, T is the absolute temperature, assumed a constant in this study, and $\kappa_{\rho_i\rho_j}, i, j = 1,2$ are model parameters measuring the strength of the conformational entropy (which are assumed constants in this study).

Sometimes, we have to use molar densities n_i as the fundamental variables in the model $i = 1,2$, system (2.16) can be rewritten as follows

$$\begin{cases}m_1(\frac{\partial n_1}{\partial t} + \nabla\cdot(n_1\mathbf{v})) = \nabla\cdot M_1\cdot\nabla(\frac{1}{m_1}\mu_{n1} - \frac{1}{m_2}\mu_{n2}),\\ m_2(\frac{\partial n_2}{\partial t} + \nabla\cdot(n_2\mathbf{v})) = -\nabla\cdot M_1\cdot\nabla(\frac{1}{m_1}\mu_{n1} - \frac{1}{m_2}\mu_{n2}),\\ \frac{\partial(\rho\mathbf{v})}{\partial t} + \nabla\cdot(\rho\mathbf{vv}) = 2\nabla\cdot(\eta\mathbf{D}) + \nabla(\overline{\eta}\nabla\cdot\mathbf{v}) - n_1\nabla\mu_{n1} - n_2\nabla\mu_{n2},\end{cases} \tag{2.19}$$

where $n_i = \frac{\rho_i}{m_i}$, m_i is the molar mass of the ith component and $\mu_{ni} = \frac{\delta f}{\delta n_i} = \frac{\delta f}{\delta \rho_i} m_i$, $i = 1, 2$. Correspondingly, the shear and volumetric viscosities are given respectively by $\eta = \sum_{i=1}^{2} \frac{n_i m_i}{n_1 m_1 + n_2 m_2} \eta_i$ and $\overline{\eta} = \sum_{i=1}^{2} \frac{n_i m_i}{n_1 m_1 + n_2 m_2} \overline{\eta_i}$.

With molar densities $n_i, i = 1, 2$ as the primitive variables, we rewrite free energy density f as follows

$$\begin{aligned} &f(n_1 m_1, n_2 m_2, m_1 \nabla n_1, m_2 \nabla n_2, T) = h(m_1 n_1, m_2 n_2, T) \\ &+ \tfrac{1}{2}[\kappa_{n_1 n_1} (\nabla n_1)^2 + 2\kappa_{n_1 n_2} (\nabla n_1, \nabla n_2) + \kappa_{n_2 n_2} (\nabla n_2)^2], \end{aligned} \tag{2.20}$$

where $\kappa_{n_i n_i} = m_i^2 \kappa_{\rho_i \rho_i}$, $i = 1, 2$ and $\kappa_{n_1 n_2} = m_1 m_2 \kappa_{\rho_1 \rho_2}$.

The free energy density function is specific to the binary fluid system studied.

- For polymeric binary fluid mixtures while approximated as a viscous fluid, the Flory-Huggins type free energy density function can be used to describe fluid mixing [13,17,35]

$$h(\rho_1, \rho_2, T) = \frac{k_B T}{m} \rho \left(\frac{1}{N_1} \frac{\rho_1}{\rho} ln \frac{\rho_1}{\rho} + \frac{1}{N_2} \frac{\rho_2}{\rho} ln \frac{\rho_2}{\rho} + \chi \frac{\rho_1 \rho_2}{\rho^2} \right), \tag{2.21}$$

  where k_B is the Boltzmann constant, T is the absolute temperature and m the average mass of a molecule.
- For compressible gas-liquid mixtures, the semi-empirical Peng-Robinson free energy density is often used [28],

$$h(n_1, n_2, \cdots, n_N, n, T) = f^{ideal} + f^{repulsion} + f^{attraction}, \tag{2.22}$$

  where

$$\begin{aligned} f^{ideal} &= RT \textstyle\sum_{i=1} n_i (ln(n_i) - 1), \\ f^{repulsion} &= -nRT ln(1 - bn), \\ f^{attraction} &= \frac{a(T) n}{2\sqrt{2} b} ln\left(\frac{1 + (1 - \sqrt{2}) bn}{1 + (1 + \sqrt{2}) bn} \right). \end{aligned} \tag{2.23}$$

  Here $n = \sum_{i=1}^{N} n_i$ is the total molar density. The corresponding chemical potential of the ith component is given by

$$\begin{aligned} \mu_{ni} &= \frac{\partial h}{\partial n_i} - \nabla \cdot \frac{\partial h}{\partial \nabla n_i} = RT\left(ln(n_i) + \frac{b_i n}{1 - bn} - ln(1 - bn) \right) + \frac{a b_i n}{b((\sqrt{2} - 1) bn - 1)(1 + (1 + \sqrt{2}) bn)} \\ &+ \frac{1}{2\sqrt{2}} \left(\frac{2 \sum_{j=1}^{M} n_j (a_i a_j)^{1/2} (1 - k_{ij})}{bn} - \frac{a b_i}{b^2} \right) ln\left(\frac{1 + (1 - \sqrt{2}) bn}{1 + (1 + \sqrt{2}) bn} \right) - \kappa_{n_i n_i} \Delta n_i - \kappa_{n_i n_j} \Delta n_j, \qquad j \neq i, \end{aligned} \tag{2.24}$$

  where $b(n_1, n_2)$ is the volume parameter and $a(n_1, n_2, T)$ is the interaction parameter. This free energy was proposed to improve that of the Van der Waals' to mitigate the deviation away from the ideal gas model.

3. Non-dimensionalization

For system (2.16), using characteristic time t_0, characteristic length l_0, and characteristic density ρ_0, we nondimensionalize the physical variables and parameters as follows

$$\begin{aligned} &\tilde{t} = \frac{t}{t_0}, \quad \tilde{x} = \frac{x}{l_0}, \quad \tilde{\rho}_i = \frac{\rho_i}{\rho_0}, \quad i = 1, 2, \quad \tilde{\mathbf{v}} = \frac{\mathbf{v} t_0}{l_0}, \quad \tilde{M}_1 = \frac{M_1}{t_0 \rho_0}, \quad \frac{1}{Re_s} = \tilde{\eta} = \frac{t_0}{\rho_0 l_0^2} \eta, \\ &\frac{1}{Re_v} = \tilde{\overline{\eta}} = \frac{t_0}{\rho_0 l_0^2} \overline{\eta}, \quad \tilde{\mu}_i = \frac{t_0^2}{l_0^2} \mu_i, \quad i = 1, 2, \quad \tilde{\kappa}_{\rho_i \rho_j} = \kappa_{\rho_i \rho_j} \frac{\rho_0 t_0^2}{l_0^4}, \quad i, j = 1, 2, \end{aligned} \tag{3.1}$$

where Re_s, Re_v are the Reynolds numbers. We rewrite the dimensionless governing equations, after dropping the $\tilde{s}$ for simplicity, as follows

$$\begin{cases} \frac{\partial \rho_1}{\partial t} + \nabla \cdot (\rho_1 \mathbf{v}) = \nabla \cdot M_1 \cdot \nabla(\mu_1 - \mu_2), \\ \frac{\partial \rho_2}{\partial t} + \nabla \cdot (\rho_2 \mathbf{v}) = -\nabla \cdot M_1 \cdot \nabla(\mu_1 - \mu_2), \\ \frac{\partial (\rho \mathbf{v})}{\partial t} + \nabla \cdot (\rho \mathbf{v} \mathbf{v}) = 2\nabla \cdot \left(\frac{1}{Re_s} \mathbf{D} \right) + \nabla \left(\frac{1}{Re_v} \nabla \cdot \mathbf{v} \right) - \rho_1 \nabla \mu_1 - \rho_2 \nabla \mu_2, \end{cases} \tag{3.2}$$

where

$$\mu_1 = \frac{\partial h}{\partial \rho_1} - \kappa_{\rho_1 \rho_1} \Delta \rho_1 - \kappa_{\rho_1 \rho_2} \Delta \rho_2, \qquad \mu_2 = \frac{\partial h}{\partial \rho_2} - \kappa_{\rho_1 \rho_2} \Delta \rho_1 - \kappa_{\rho_2 \rho_2} \Delta \rho_2. \tag{3.3}$$

Similarly, for system (2.19) with molar density as fundamental variables, using characteristic molar density n_0 $(mol \cdot m^{-d})$, characteristic mass density $\rho_0 = n_0 m_2 (kg \cdot m^{-d}, d = 3)$ and characteristic temperature T_0 (Kelvin), we nondimensionalize the physical variables and parameters as follows

$$\begin{aligned}
&\tilde{t}=\frac{t}{t_0},\quad \tilde{x}=\frac{x}{l_0},\quad \tilde{\rho}=\frac{\rho}{\rho_0},\quad \tilde{n}=\frac{n}{n_0},\quad \tilde{T}=\frac{T}{T_0},\quad \frac{1}{Re_s}=\tilde{\eta}=\frac{t_0}{\rho_0 l_0^2}\eta,\quad \tilde{m_1}=\frac{m_1 n_0}{\rho_0},\quad \tilde{m_2}=\frac{m_2 n_0}{\rho_0},\\
&\frac{1}{Re_v}=\tilde{\overline{\eta}}=\frac{t_0}{\rho_0 l_0^2}\overline{\eta},\quad \tilde{\mu}_{ni}=\frac{n_0 t_0^2}{\rho_0 l_0^2}\mu_{ni},\quad i=1,2,\quad \tilde{M}_1=\frac{M_1}{t_0\rho_0},\quad \tilde{\kappa_{n_i n_j}}=\kappa_{n_i n_j}\frac{n_0^2 t_0^2}{\rho_0 l_0^4},\quad i,j=1,2.
\end{aligned}\tag{3.4}$$

Dropping ~s for simplicity, we rewrite the dimensionless governing equations as follows

$$\begin{cases}
m_1(\frac{\partial n_1}{\partial t}+\nabla\cdot(n_1\mathbf{v}))=\nabla\cdot M_1\cdot\nabla(\frac{1}{m_1}\mu_{n1}-\mu_{n2}),\\
(\frac{\partial n_2}{\partial t}+\nabla\cdot(n_2\mathbf{v}))=-\nabla\cdot M_1\cdot\nabla(\frac{1}{m_1}\mu_{n1}-\mu_{n2}),\\
\frac{\partial(\rho\mathbf{v})}{\partial t}+\nabla\cdot(\rho\mathbf{v}\mathbf{v})=2\nabla\cdot(\eta\mathbf{D})+\nabla(\overline{\eta}\nabla\cdot\mathbf{v})-n_1\nabla\mu_{n1}-n_2\nabla\mu_{n2},
\end{cases}\tag{3.5}$$

where we set $\tilde{m_2}=\frac{m_2 n_0}{\rho_0}=1$, then m_1 is the ratio of the specific masses, a dimensionless model parameter. The dimensionless chemical potentials are given by

$$\mu_{n1}=\frac{\partial h}{\partial n_1}-\kappa_{n_1n_1}\Delta n_1-\kappa_{n_1n_2}\Delta n_2,\qquad \mu_{n2}=\frac{\partial h}{\partial n_2}-\kappa_{n_1n_2}\Delta n_1-\kappa_{n_2n_2}\Delta n_2.\tag{3.6}$$

In the following, we focus on developing an energy stable numerical scheme for system (3.2) on staggered grids in space. An energy stable numerical scheme for system (3.5) can be obtained analogously, but we will not present it in this paper.

4. Reformulation of the model

In order to use the Energy Quadratization (EQ) method to design numerical schemes, we need to reformulate the model equations. We first transform the energy of the system into a quadratic form

$$\begin{aligned}
&E=\int_V[\tfrac{1}{2}\rho\mathbf{v}^T\mathbf{v}+f]d\mathbf{x}=\int_V[\tfrac{1}{2}\mathbf{u}^T\mathbf{u}+f_u]d\mathbf{x},\\
&f_u=q_1^2+\tfrac{\alpha_1}{2}\rho_1^2+\tfrac{\alpha_2}{2}\rho_2^2+\tfrac{1}{2}\mathbf{p}^T\cdot\mathbf{K}\cdot\mathbf{p}-A,
\end{aligned}\tag{4.1}$$

where $\mathbf{u}=\sqrt{\rho}\mathbf{v}$, $\alpha_1>0$ and $\alpha_2>0$ are two user-defined parameters,

$$q_1=\sqrt{h(\rho_1,\rho_2,T)-\frac{\alpha_1}{2}\rho_1^2-\frac{\alpha_2}{2}\rho_2^2+A},\tag{4.2}$$

and A is a constant such that $h(\rho_1,\rho_2,T)-\frac{\alpha_1}{2}\rho_1^2-\frac{\alpha_2}{2}\rho_2^2+A>0$. We note that we can always find a constant A if the bulk free energy density function is bounded below. In addition, $\mathbf{p}=(\nabla\rho_1,\nabla\rho_2)^T$ and $\mathbf{K}$ is the coefficient matrix of the conformational entropy

$$\mathbf{K}=\begin{pmatrix}\kappa_{\rho_1\rho_1} & \kappa_{\rho_1\rho_2}\\ \kappa_{\rho_1\rho_2} & \kappa_{\rho_2\rho_2}\end{pmatrix}>0.\tag{4.3}$$

Using identity

$$\frac{\partial(\sqrt{\rho}\mathbf{u})}{\partial t}=\frac{1}{2\sqrt{\rho}}\frac{\partial\rho}{\partial t}\mathbf{u}+\sqrt{\rho}\frac{\partial\mathbf{u}}{\partial t}=-\frac{1}{2\sqrt{\rho}}\nabla\cdot(\sqrt{\rho}\mathbf{u})\mathbf{u}+\sqrt{\rho}\frac{\partial\mathbf{u}}{\partial t},\tag{4.4}$$

we rewrite the governing equations into

$$\begin{cases}
\frac{\partial\rho_1}{\partial t}+\nabla\cdot(\frac{\rho_1}{\sqrt{\rho}}\mathbf{u})=\nabla\cdot M_1\cdot\nabla(\mu_1-\mu_2),\\
\frac{\partial\rho_2}{\partial t}+\nabla\cdot(\frac{\rho_2}{\sqrt{\rho}}\mathbf{u})=-\nabla\cdot M_1\cdot\nabla(\mu_1-\mu_2),\\
\frac{\partial\mathbf{u}}{\partial t}+\frac{1}{2}(\frac{1}{\sqrt{\rho}}\nabla\cdot(\mathbf{u}\mathbf{u})+\mathbf{u}\cdot\nabla\frac{\mathbf{u}}{\sqrt{\rho}})=\frac{1}{\sqrt{\rho}}\nabla\cdot\sigma,\\
\frac{\partial q_1}{\partial t}=\frac{\partial q_1}{\partial\rho_1}\frac{\partial\rho_1}{\partial t}+\frac{\partial q_1}{\partial\rho_2}\frac{\partial\rho_2}{\partial t},
\end{cases}\tag{4.5}$$

where

$$
\begin{aligned}
&\sigma = \sigma^s + \sigma^e, \quad \sigma^s = 2\tfrac{1}{Re_s}\mathbf{D} + \tfrac{1}{Re_v}(\nabla\cdot\tfrac{\mathbf{u}}{\sqrt{\rho}})\mathbf{I},\\
&\sigma^e = (f - \rho_1\mu_1 - \rho_2\mu_2)\mathbf{I} - \tfrac{\partial f}{\partial\nabla\rho_1}\nabla\rho_1 - \tfrac{\partial f}{\partial\nabla\rho_2}\nabla\rho_2,\\
&\nabla\cdot\sigma = \nabla\cdot(\sigma^s+\sigma^e) = 2\nabla\cdot(\tfrac{1}{Re_s}\mathbf{D}) + \nabla(\tfrac{1}{Re_v}\nabla\cdot\tfrac{\mathbf{u}}{\sqrt{\rho}}) - \rho_1\nabla\mu_1 - \rho_2\nabla\mu_2,\\
&\mu_1 = \tfrac{\delta f}{\delta\rho_1} = \tfrac{\partial f_u}{\partial\rho_1} - \nabla\cdot\tfrac{\partial f_u}{\partial\nabla\rho_1} = 2q_1\tfrac{\partial q_1}{\partial\rho_1} - \kappa_{\rho_1\rho_1}\Delta\rho_1 - \kappa_{\rho_1\rho_2}\Delta\rho_2 + \alpha_1\rho_1,\\
&\mu_2 = \tfrac{\delta f}{\delta\rho_2} = \tfrac{\partial f_u}{\partial\rho_2} - \nabla\cdot\tfrac{\partial f_u}{\partial\nabla\rho_2} = 2q_1\tfrac{\partial q_1}{\partial\rho_2} - \kappa_{\rho_2\rho_2}\Delta\rho_2 - \kappa_{\rho_1\rho_2}\Delta\rho_1 + \alpha_2\rho_2,\\
&\mathbf{D} = \tfrac{1}{2}(\nabla\tfrac{\mathbf{u}}{\sqrt{\rho}} + (\nabla\tfrac{\mathbf{u}}{\sqrt{\rho}})^T), \quad \tfrac{1}{Re_s} = \tfrac{\rho_1}{\rho}\tfrac{1}{Re_{s1}} + \tfrac{\rho_2}{\rho}\tfrac{1}{Re_{s2}}, \quad \tfrac{1}{Re_v} = \tfrac{\rho_1}{\rho}\tfrac{1}{Re_{v1}} + \tfrac{\rho_2}{\rho}\tfrac{1}{Re_{v2}}.
\end{aligned}
\tag{4.6}
$$

Remark 4.1. We define the inner product of two functions f and g as follows:

$$
(f,g) = \int_V fg d\mathbf{x}. \tag{4.7}
$$

Remark 4.2. In (4.5), $\mathbf{u}$ is well defined only when $\rho > 0$. Therefore, we note that the reformulated system should not be applied to the case where $\rho = 0$.

Theorem 4.1. *System (4.5) is dissipative, and the corresponding energy dissipation rate is given by*

$$
\tfrac{dE}{dt} = -2(\tfrac{1}{Re_s}, \mathbf{D}:\mathbf{D}) - (\tfrac{1}{Re_v}\nabla\cdot\tfrac{\mathbf{u}}{\sqrt{\rho}}, \nabla\cdot\tfrac{\mathbf{u}}{\sqrt{\rho}}) - (\nabla\mu_1, \nabla\mu_2)\cdot\mathcal{M}\cdot(\nabla\mu_1, \nabla\mu_2)^T \le 0, \tag{4.8}
$$

where $Re_s, Re_v \ge 0$, $\mathcal{M} = \begin{pmatrix} M_1 & -M_1 \\ -M_1 & M_1 \end{pmatrix} \ge 0$.

Proof. By the definition of E, we have

$$
\begin{aligned}
&\tfrac{\partial E}{\partial t} = \int_V \left[\mathbf{u}^T\tfrac{\partial\mathbf{u}}{\partial t} + 2q_1\tfrac{\partial q_1}{\partial t} + \alpha_1\rho_1\tfrac{\partial\rho_1}{\partial t} + \alpha_2\rho_2\tfrac{\partial\rho_2}{\partial t} + (\nabla\rho_1, \nabla\rho_2)\cdot\mathbf{K}\cdot(\nabla\tfrac{\partial\rho_1}{\partial t}, \nabla\tfrac{\partial\rho_2}{\partial t})^T\right]d\mathbf{x}\\
&= (\mathbf{u}, \tfrac{\partial\mathbf{u}}{\partial t}) + 2(q_1, \tfrac{\partial q_1}{\partial t}) + ((\mu_1 - 2q_1\tfrac{\partial q_1}{\partial\rho_1}), \tfrac{\partial\rho_1}{\partial t}) + ((\mu_2 - 2q_1\tfrac{\partial q_1}{\partial\rho_2}), \tfrac{\partial\rho_2}{\partial t})\\
&= (\mathbf{u}, \tfrac{\partial\mathbf{u}}{\partial t}) + 2(q_1, \tfrac{\partial q_1}{\partial t} - q_1\tfrac{\partial q_1}{\partial\rho_1}\tfrac{\partial\rho_1}{\partial t} - q_1\tfrac{\partial q_1}{\partial\rho_2}), \tfrac{\partial\rho_2}{\partial t}) + (\mu_1, \tfrac{\partial\rho_1}{\partial t}) + (\mu_2, \tfrac{\partial\rho_2}{\partial t})\\
&= (\mathbf{u}, \tfrac{\partial\mathbf{u}}{\partial t}) + (\mu_1, \tfrac{\partial\rho_1}{\partial t}) + (\mu_2, \tfrac{\partial\rho_2}{\partial t}).
\end{aligned}
\tag{4.9}
$$

Taking the inner product of (4.5-3) with $\mathbf{u}$ and using integration by parts, we obtain

$$
(\mathbf{u}, \tfrac{\partial\mathbf{u}}{\partial t}) = -2(\tfrac{1}{Re_s}, \mathbf{D}:\mathbf{D}) - (\tfrac{1}{Re_v}\nabla\cdot\tfrac{\mathbf{u}}{\sqrt{\rho}}, \nabla\cdot\tfrac{\mathbf{u}}{\sqrt{\rho}}) - (\mathbf{u}, \rho_1\tfrac{1}{\sqrt{\rho}}\nabla\mu_1 + \rho_2\tfrac{1}{\sqrt{\rho}}\nabla\mu_2). \tag{4.10}
$$

Taking the inner product of (4.5-1,2) with μ_1, μ_2, respectively, and performing integration by parts, we obtain

$$
\begin{aligned}
&(\mu_1, \tfrac{\partial\rho_1}{\partial t}) + (\mu_2, \tfrac{\partial\rho_2}{\partial t}) = -[\nabla(\mu_1 - \mu_2)M_1\nabla(\mu_1 - \mu_2)] + (\mathbf{u}, \rho_1\tfrac{1}{\sqrt{\rho}}\nabla\mu_1 + \rho_2\tfrac{1}{\sqrt{\rho}}\nabla\mu_2)\\
&= -(\nabla\mu_1, \nabla\mu_2)\cdot\mathcal{M}\cdot(\nabla\mu_1, \nabla\mu_2)^T + (\mathbf{u}, \rho_1\tfrac{1}{\sqrt{\rho}}\nabla\mu_1 + \rho_2\tfrac{1}{\sqrt{\rho}}\nabla\mu_2).
\end{aligned}
\tag{4.11}
$$

Combining (4.10) and (4.11), we obtain

$$
\tfrac{\partial E}{\partial t} = -2(\tfrac{1}{Re_s}, \mathbf{D}:\mathbf{D}) - (\tfrac{1}{Re_v}\nabla\cdot\tfrac{\mathbf{u}}{\sqrt{\rho}}, \nabla\cdot\tfrac{\mathbf{u}}{\sqrt{\rho}}) - (\nabla\mu_1, \nabla\mu_2)\cdot\mathcal{M}\cdot(\nabla\mu_1, \nabla\mu_2)^T \le 0 \tag{4.12}
$$

provided $\mathcal{M} \ge 0$. □

We next design a second order energy stable numerical scheme based on the reformulated governing system of equations.

5. Linear, second order energy stable numerical scheme

5.1. Notations and useful lemmas

We first introduce some notations, finite difference operators and useful lemmas. Here, we follow the notations in [11, 20]. Similar notations have also been used in [9,23,45,50]. Let $\Omega = [0, L_x] \times [0, L_y]$ be the computational domain with

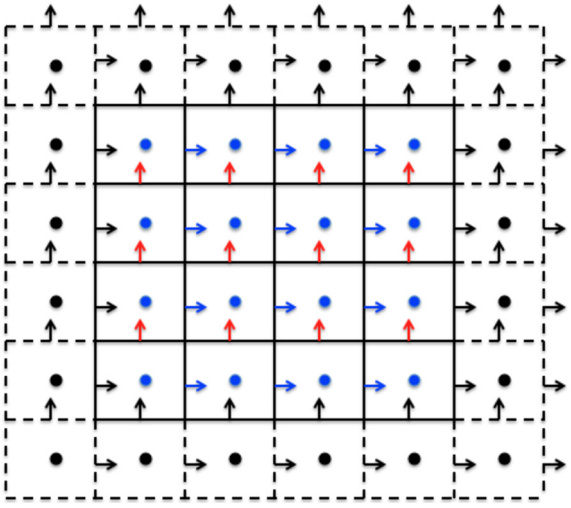

Fig. 5.1. Staggered grid in 2D space. (For interpretation of the colors in the figure(s), the reader is referred to the web version of this article.)

$L_x = h_x \times N_x$, $L_y = h_y \times N_y$, where N_x, N_y are positive integers, and h_x, h_y are spatial step sizes in the x and y direction, respectively. We define three sets for the grid points as follows

$$\begin{aligned} E_x &:= \{x_{i+1/2} = i \cdot h \quad | \quad i = 0, 1, \cdots, N_x\}, \\ C_x &:= \{x_i = (i - \tfrac{1}{2}) \cdot h \quad | \quad i = 1, \cdots, N_x\}, \\ C_{\overline{x}} &:= \{x_i = (i - \tfrac{1}{2}) \cdot h \quad | \quad i = 0, 1, \cdots, N_x, N_x + 1\}, \end{aligned} \tag{5.1}$$

where E_x is a uniform partition of $[0, L_x]$ of size N_x in the x-direction and its elements are called edge-centered points. The elements of C_x and $C_{\overline{x}}$ are called cell-centered points. The two points belonging to $C_{\overline{x}} \backslash C_x$ are called ghost points. Analogously, we define E_y as the uniform partition of $[0, L_y]$ of size N_y, called edge-centered points in the y-direction, and $C_y, C_{\overline{y}}$ the cell-centered points of the interval $[0, L_y]$. In Fig. 5.1, we show the staggered grid in 2D space. In this paper, we discretize the variables with the Neumann boundary conditions at the cell-center and the ones with the Dirichlet boundary conditions at the edge-center. We define the corresponding discrete function space on this staggered grid as follows

$$\begin{aligned} &\mathcal{C}_{x\times y} := \{\phi : C_x \times C_y \to \mathcal{R}\}, \quad \mathcal{C}_{\overline{x}\times y} := \{\phi : C_{\overline{x}} \times C_y \to \mathcal{R}\}, \quad \mathcal{C}_{x\times \overline{y}} := \{\phi : C_x \times C_{\overline{y}} \to \mathcal{R}\}, \\ &\mathcal{C}_{\overline{x}\times \overline{y}} := \{\phi : C_{\overline{x}} \times C_{\overline{y}} \to \mathcal{R}\}, \quad \mathcal{E}^{ew}_{x\times y} := \{\phi : E_x \times C_y \to \mathcal{R}\}, \quad \mathcal{E}^{ew}_{x\times \overline{y}} := \{\phi : E_x \times C_{\overline{y}} \to \mathcal{R}\}, \\ &\mathcal{E}^{ns}_{x\times y} := \{\phi : C_x \times E_y \to \mathcal{R}\}, \quad \mathcal{E}^{ns}_{\overline{x}\times y} := \{\phi : C_{\overline{x}} \times E_y \to \mathcal{R}\}, \quad \mathcal{V}_{x\times y} := \{\phi : E_x \times E_y \to \mathcal{R}\}. \end{aligned} \tag{5.2}$$

$\mathcal{C}_{x\times y}, \mathcal{C}_{\overline{x}\times y}, \mathcal{C}_{x\times \overline{y}}$ and $\mathcal{C}_{\overline{x}\times \overline{y}}$ are the sets for discrete cell-centered functions, and $\mathcal{E}^{ew}_{x\times y}, \mathcal{E}^{ns}_{x\times y}$ east-west and north-south edge-centered functions, respectively.

5.1.1. Average and difference operators

Assume $u, r \in \mathcal{E}^{ew}_{x\times y} \cup \mathcal{E}^{ew}_{x\times \overline{y}}$, $v, w \in \mathcal{E}^{ns}_{x\times y} \cup \mathcal{E}^{ns}_{\overline{x}\times y}$, $\phi, \psi \in \mathcal{C}_{x\times y} \cup \mathcal{C}_{\overline{x}\times y} \cup \mathcal{C}_{x\times \overline{y}} \cup \mathcal{C}_{\overline{x}\times \overline{y}}$ and $f \in \mathcal{V}_{x\times y}$, we define the east-west-edge-to-center average and difference operator as $a_x, d_x : \mathcal{E}^{ew}_{x\times \overline{y}} \cup \mathcal{V}_{x\times y} \to \mathcal{C}_{x\times \overline{y}} \cup \mathcal{E}^{ns}_{x\times y}$ component-wise as follows

$$\begin{aligned} a_x u_{i,j} &:= \tfrac{1}{2}(u_{i+\frac{1}{2},j} + u_{i-\frac{1}{2},j}), \quad d_x u_{i,j} := \tfrac{1}{h_x}(u_{i+\frac{1}{2},j} - u_{i-\frac{1}{2},j}), \\ a_x f_{i,j+\frac{1}{2}} &:= \tfrac{1}{2}(f_{i+\frac{1}{2},j+\frac{1}{2}} + f_{i-\frac{1}{2},j+\frac{1}{2}}), \quad d_x f_{i,j+\frac{1}{2}} := \tfrac{1}{h_x}(f_{i+\frac{1}{2},j+\frac{1}{2}} - f_{i-\frac{1}{2},j+\frac{1}{2}}). \end{aligned} \tag{5.3}$$

The north-south-edge-to-center average and difference operators are defined as $a_y, d_y : \mathcal{E}^{ns}_{\overline{x}\times y} \cup \mathcal{V}_{x\times y} \to \mathcal{C}_{\overline{x}\times y} \cup \mathcal{E}^{ew}_{x\times y}$ component-wise as follows

$$\begin{aligned} a_y v_{i,j} &:= \tfrac{1}{2}(v_{i,j+\frac{1}{2}} + v_{i,j-\frac{1}{2}}), \quad d_y v_{i,j} := \tfrac{1}{h_y}(v_{i,j+\frac{1}{2}} - v_{i,j-\frac{1}{2}}), \\ a_y f_{i+\frac{1}{2},j} &:= \tfrac{1}{2}(f_{i+\frac{1}{2},j+\frac{1}{2}} + f_{i+\frac{1}{2},j-\frac{1}{2}}), \quad d_y f_{i+\frac{1}{2},j} := \tfrac{1}{h_y}(f_{i+\frac{1}{2},j+\frac{1}{2}} - f_{i+\frac{1}{2},j-\frac{1}{2}}). \end{aligned} \tag{5.4}$$

We denote the center-to-east-west-edge average and difference operators as $A_x, D_x : \mathcal{C}_{\overline{x}\times \overline{y}} \cup \mathcal{E}^{ns}_{\overline{x}\times y} \to \mathcal{E}^{ew}_{x\times \overline{y}} \cup \mathcal{V}_{x\times y}$ in component-wise forms:

$$A_x\phi_{i+\frac{1}{2},j} := \tfrac{1}{2}(\phi_{i+1,j}+\phi_{i,j}), \quad D_x\phi_{i+\frac{1}{2},j} := \tfrac{1}{h_x}(\phi_{i+1,j}-\phi_{i,j}),$$
$$A_x v_{i+\frac{1}{2},j+\frac{1}{2}} := \tfrac{1}{2}(v_{i+1,j+\frac{1}{2}}+v_{i,j+\frac{1}{2}}), \quad D_x v_{i+\frac{1}{2},j+\frac{1}{2}} := \tfrac{1}{h_x}(v_{i+1,j+\frac{1}{2}}-v_{i,j+\frac{1}{2}}). \tag{5.5}$$

Analogously, the center-to-north-south-edge average and difference operator are defined as $A_y, D_y : \mathcal{C}_{\overline{x}\times\overline{y}} \cup \mathcal{E}^{ew}_{x\times\overline{y}} \to \mathcal{E}^{ns}_{\overline{x}\times y} \cup \mathcal{V}_{x\times y}$ in component-wise forms:

$$A_y\phi_{i,j+\frac{1}{2}} := \tfrac{1}{2}(\phi_{i,j+1}+\phi_{i,j}), \quad D_y\phi_{i,j+\frac{1}{2}} := \tfrac{1}{h_y}(\phi_{i,j+1}-\phi_{i,j}),$$
$$A_y u_{i+\frac{1}{2},j+\frac{1}{2}} := \tfrac{1}{2}(u_{i+\frac{1}{2},j+1}+u_{i+\frac{1}{2},j}), \quad D_y u_{i+\frac{1}{2},j+\frac{1}{2}} := \tfrac{1}{h_y}(u_{i+\frac{1}{2},j+1}-u_{i+\frac{1}{2},j}). \tag{5.6}$$

The standard 2D discrete Laplace operator is defined as $\Delta_h : \mathcal{E}^{ew}_{x\times\overline{y}} \cup \mathcal{E}^{ns}_{\overline{x}\times y} \cup \mathcal{C}_{\overline{x}\times\overline{y}} \to \mathcal{E}^{ew}_{x\times y} \cup \mathcal{E}^{ns}_{x\times y} \cup \mathcal{C}_{x\times y}$:

$$\Delta_h u := D_x(d_x u) + d_y(D_y u), \quad \Delta_h v := d_x(D_x v) + D_y(d_y v), \quad \Delta_h\phi := d_x(D_x\phi) + d_y(D_y\phi). \tag{5.7}$$

5.1.2. Boundary conditions

The homogenous Neumann boundary conditions of ϕ ($\phi = \rho_i, \mu_i, i = 1, 2$) are discretized as follows

$$\phi_{0,j} = \phi_{1,j}, \quad \phi_{N_x,j} = \phi_{N_x+1,j}, \quad j = 0, 1, 2, \cdots, N_y+1,$$
$$\phi_{i,0} = \phi_{i,1}, \quad \phi_{i,N_y} = \phi_{i,N_y+1}, \quad i = 0, 1, 2, \cdots, N_x+1. \tag{5.8}$$

We denote it as $\mathbf{n}\cdot\nabla_h\phi|_{\partial V} = 0$.

The homogeneously Dirichlet boundary conditions of $\mathbf{v} = (u, v)$ are discretized as follows

$$u_{\frac{1}{2},j} = u_{N_x+\frac{1}{2},j} = 0, \quad j = 1, 2, \cdots, N_y,$$
$$A_y u_{i+\frac{1}{2},\frac{1}{2}} = A_y u_{i+\frac{1}{2},N_y+\frac{1}{2}} = 0, \quad i = 0, 1, 2, \cdots, N_x,$$
$$v_{i,\frac{1}{2}} = v_{i,N_y+\frac{1}{2}} = 0, \quad j = 1, 2, \cdots, N_x,$$
$$A_x v_{\frac{1}{2},j+\frac{1}{2}} = A_x v_{N_x+\frac{1}{2},j+\frac{1}{2}} = 0, \quad j = 0, 1, 2, \cdots, N_y. \tag{5.9}$$

We denote it as $u_h|_{\partial V} = 0$ and $v_h|_{\partial V} = 0$.

If $f \in \mathcal{V}_{x\times y}$ satisfies homogenous Dirichlet boundary condition, we have

$$f_{\frac{1}{2},j+\frac{1}{2}} = f_{N_x+\frac{1}{2},j+\frac{1}{2}} = f_{i+\frac{1}{2},\frac{1}{2}} = f_{i+\frac{1}{2},N_y+\frac{1}{2}} = 0, \tag{5.10}$$

where $i = 0, 1, 2, \cdots, N_x$, $j = 0, 1, 2, \cdots, N_y$. We denote is as $f_h|_{\partial V} = 0$.

5.1.3. Inner products and norms

We defined the inner products for discrete functions as follows

$$(\phi,\psi)_2 := h_x h_y \sum_{i=1}^{N_x}\sum_{j=1}^{N_y}\phi_{i,j}\psi_{i,j}, \quad [u,r]_{ew} := (a_x(ur),1)_2, \quad [v,w]_{ns} := (a_y(uw),1)_2,$$
$$(f,g)_{vc} := (a_x(a_y(fg)),1)_2, \quad (\nabla\phi,\nabla\psi)_h := [D_x(\phi), D_x(\psi)]_{ew} + [D_y(\phi), D_y(\psi)]_{ns}. \tag{5.11}$$

The corresponding norms are defined by

$$\|\phi\|_2 := (\phi,\phi)_2^{\frac{1}{2}}, \quad \|u\|_{ew} := [u,u]_{ew}^{\frac{1}{2}}, \quad \|v\|_{ns} := [v,v]_{ns}^{\frac{1}{2}}, \quad \|f\|_{vc} := (f,f)_{vc}^{\frac{1}{2}}. \tag{5.12}$$

For $\phi = \mathcal{C}_{\overline{x}\times\overline{y}}$, we define $\|\nabla\phi\|_2$ as

$$\|\nabla\phi\|_2 := \sqrt{\|D_x\phi\|_{ew}^2 + \|D_y\phi\|_{ns}^2}. \tag{5.13}$$

For the edge-centered velocity vector $\mathbf{v} = (u, v)$, $u \in \mathcal{E}^{ew}_{x\times\overline{y}}$, $v \in \mathcal{E}^{ns}_{\overline{x}\times y}$, we define $\|\mathbf{v}\|_2, \|\nabla\mathbf{v}\|_2$ as

$$\|\mathbf{v}\|_2 := \sqrt{\|u\|_{ew}^2 + \|v\|_{ns}^2}, \quad \|\nabla\mathbf{v}\|_2 := \sqrt{\|d_x u\|_2^2 + \|D_y u\|_{vc}^2 + \|D_x v\|_{vc}^2 + \|d_y v\|_2^2},$$
$$\|\mathbf{D}\|_2 := \sqrt{\|d_x u\|_2^2 + \tfrac{1}{2}\|D_y u\|_{vc}^2 + \tfrac{1}{2}\|D_x v\|_{vc}^2 + (D_y u, D_x v)_{vc} + \|d_y v\|_2^2},$$
$$(\phi, \mathbf{D}:\mathbf{D})_2 :=$$
$$\sqrt{(\phi,(d_x u)^2)_2 + \tfrac{1}{2}(A_x(A_y\phi),(D_y u)^2)_{vc} + \tfrac{1}{2}(A_x(A_y\phi),(D_x v)^2)_{vc} + (A_x(A_y\phi)D_y u, D_x v)_{vc} + (\phi,(d_y v)^2)_2}, \tag{5.14}$$

where $\mathbf{D} = \frac{1}{2}(\nabla\mathbf{v} + \nabla\mathbf{v}^T)$. From these definitions, we obtain the following lemmas [20]:

Lemma 5.1. *(Summation by parts): If $\phi \in \mathcal{C}_{\overline{x}\times\overline{y}}$, $u \in \mathcal{E}^{ew}_{x\times y}$, $v \in \mathcal{E}^{ns}_{x\times y}$, and $u_h|_{\partial V} = 0$ and $v_h|_{\partial V} = 0$, then*

$$\begin{aligned} &[A_x\phi, u]_{ew} = (\phi, a_x u)_2, \quad [A_y\phi, v]_{ns} = (\phi, a_y v)_2, \\ &[D_x\phi, u]_{ew} + (\phi, d_x u)_2 = 0, \quad [D_y\phi, v]_{ns} + (\phi, d_y v)_2 = 0, \end{aligned} \tag{5.15}$$

Lemma 5.2. *If $f \in \mathcal{V}_{x\times y}$, and $f_h|_{\partial V} = 0$, $u \in \mathcal{E}^{ew}_{x\times\overline{y}}$, $v \in \mathcal{E}^{ns}_{\overline{x}\times y}$, then*

$$[a_y f, u]_{ew} = (f, A_y u)_{vc}, \quad [a_x f, v]_{ns} = (f, A_x v)_{vc}. \tag{5.16}$$

Lemma 5.3. *If $f \in \mathcal{V}_{x\times y}$, $u \in \mathcal{E}^{ew}_{x\times\overline{y}}$, $v \in \mathcal{E}^{ns}_{\overline{x}\times y}$, and $u_h|_{\partial V} = 0$ and $v_h|_{\partial V} = 0$, then*

$$[d_y f, u]_{ew} + (f, D_y u)_{vc} = 0, \quad [d_x f, v]_{ns} + (f, D_x v)_{vc} = 0. \tag{5.17}$$

With these notations and lemmas, we are ready to introduce the fully-discrete numerical scheme in the following section.

5.2. Semi-discrete scheme in time

First, we discretize the governing equations using Crank-Nicolson method in time. We denote

$$\delta_t(\cdot)^{n+1/2} = \tfrac{1}{\Delta t}((\cdot)^{n+1} - (\cdot)^n), \qquad \overline{(\cdot)}^{n+1/2} = \tfrac{1}{2}(3(\cdot)^n - (\cdot)^{n-1}). \tag{5.18}$$

The second order algorithm is given below.

Algorithm 1.

$$\begin{cases} \delta_t\rho_1^{n+1/2} + \nabla\cdot(\overline{\rho}_1^{n+1/2}\overline{\frac{1}{\sqrt{\rho}}}^{n+1/2}\mathbf{u}^{n+1/2}) = \nabla\cdot M_1\cdot\nabla\mu_1^{n+1/2} - \nabla\cdot M_1\cdot\nabla\mu_2^{n+1/2}, \\ \delta_t\rho_2^{n+1/2} + \nabla\cdot(\overline{\rho}_2^{n+1/2}\overline{\frac{1}{\sqrt{\rho}}}^{n+1/2}\mathbf{u}^{n+1/2}) = -\nabla\cdot M_1\cdot\nabla\mu_1^{n+1/2} + \nabla\cdot M_1\cdot\nabla\mu_2^{n+1/2}, \\ \delta_t\mathbf{u}^{n+1/2} + \frac{1}{2}(\overline{\frac{1}{\sqrt{\rho}}}^{n+1/2}\nabla\cdot(\overline{\mathbf{u}}^{n+1/2}\mathbf{u}^{n+1/2}) + \overline{\mathbf{u}}^{n+1/2}\cdot\nabla(\overline{\frac{1}{\sqrt{\rho}}}^{n+1/2}\mathbf{u}^{n+1/2})) = \\ \overline{\frac{1}{\sqrt{\rho}}}^{n+1/2}(2\nabla\cdot(\frac{1}{Re_s}\mathbf{D}^{n+1/2}) + \nabla(\frac{1}{Re_v}\nabla\cdot(\overline{\frac{1}{\sqrt{\rho}}}^{n+1/2}\mathbf{u}^{n+1/2})) - \overline{\rho_1}^{n+1/2}\nabla\mu_1^{n+1/2} \\ -\overline{\rho_2}^{n+1/2}\nabla\mu_2{}^{n+1/2}), \\ \delta_t q_1^{n+1/2} = \overline{\frac{\partial q_1}{\partial\rho_1}}^{n+1/2}\delta_t\rho_1^{n+1/2} + \overline{\frac{\partial q_1}{\partial\rho_2}}^{n+1/2}\delta_t\rho_2^{n+1/2}, \end{cases} \tag{5.19}$$

where

$$\begin{aligned} &\mu_1^{n+1/2} = 2q_1^{n+1/2}\overline{\frac{\partial q_1}{\partial\rho_1}}^{n+1/2} - \kappa_{\rho_1\rho_1}\Delta\rho_1^{n+1/2} - \kappa_{\rho_1\rho_2}\Delta\rho_2^{n+1/2} + \alpha_1\rho_1^{n+1/2}, \\ &\mu_2^{n+1/2} = 2q_1^{n+1/2}\overline{\frac{\partial q_1}{\partial\rho_2}}^{n+1/2} - \kappa_{\rho_1\rho_2}\Delta\rho_1^{n+1/2} - \kappa_{\rho_2\rho_2}\Delta\rho_2^{n+1/2} + \alpha_2\rho_2^{n+1/2}, \\ &\mathbf{D}^{n+1/2} = \tfrac{1}{2}(\nabla(\overline{\frac{1}{\sqrt{\rho}}}^{n+1/2}\mathbf{u}^{n+1/2}) + \nabla(\overline{\frac{1}{\sqrt{\rho}}}^{n+1/2}\mathbf{u}^{n+1/2})^T), \\ &\frac{1}{Re_s} = \overline{\frac{\rho_1}{\rho}}^{n+1/2}\frac{1}{Re_{s1}} + \overline{\frac{\rho_2}{\rho}}^{n+1/2}\frac{1}{Re_{s2}}, \qquad \frac{1}{Re_v} = \overline{\frac{\rho_1}{\rho}}^{n+1/2}\frac{1}{Re_{v1}} + \overline{\frac{\rho_2}{\rho}}^{n+1/2}\frac{1}{Re_{v2}}. \end{aligned} \tag{5.20}$$

Remark 5.1. Given that (4.5) is well-defined when $\rho > 0$, the above scheme should be used only in this case.

For the scheme, we have the following theorem.

Theorem 5.1. *Scheme (5.19) is unconditional energy stable, and satisfies the following discrete energy identity*

$$\begin{aligned} &\tfrac{E^{n+1}-E^n}{\Delta t} = -2(\tfrac{1}{Re_s}, \mathbf{D}^{n+1/2} : \mathbf{D}^{n+1/2}) - (\tfrac{1}{Re_v}\nabla\cdot(\overline{\tfrac{1}{\sqrt{\rho}}}^{n+1/2}\mathbf{u}^{n+1/2}), \nabla\cdot(\overline{\tfrac{1}{\sqrt{\rho}}}^{n+1/2}\mathbf{u}^{n+1/2})) \\ &-(\nabla\mu_1^{n+1/2}, \nabla\mu_2^{n+1/2})\cdot\mathcal{M}\cdot(\nabla\mu_1^{n+1/2}, \nabla\mu_2^{n+1/2})^T < 0, \end{aligned} \tag{5.21}$$

where

$$E^n = \int_V [\tfrac{1}{2}||\mathbf{u}^n||^2 + (q_1^n)^2 + \tfrac{\alpha_1}{2}(\rho_1^n)^2 + \tfrac{\alpha_2}{2}(\rho_2^n)^2 + \tfrac{1}{2}(\mathbf{p}^n)^T \cdot \mathbf{K}^n \cdot \mathbf{p}^n - A]d\mathbf{x}, \tag{5.22}$$

and $\mathbf{p}^n = (\nabla\rho_1^n, \nabla\rho_2^n)$.

Remark 5.2. We present a useful identity in the proof of the theorem as follows

$$(\mathbf{u}^{n+1/2}, \tfrac{1}{2}(\overline{\tfrac{1}{\sqrt{\rho}}}^{n+1/2}\nabla\cdot(\overline{\mathbf{u}}^{n+1/2}\mathbf{u}^{n+1/2}) + \overline{\mathbf{u}}^{n+1/2}\cdot\nabla(\overline{\tfrac{1}{\sqrt{\rho}}}^{n+1/2}\mathbf{u}^{n+1/2}))) = 0. \tag{5.23}$$

Proof. By the definition of E^n, we have

$$\begin{aligned}
&\tfrac{E^{n+1}-E^n}{\Delta t} = \int_V [\mathbf{u}^{n+1/2}\delta_t\mathbf{u}^{n+1/2} + 2q_1^{n+1/2}\delta_t q_1^{n+1/2} + \kappa_{\rho_1\rho_1}\nabla\rho^{n+1/2}\delta_t\nabla\rho_1^{n+1/2} \\
&+\kappa_{\rho_2\rho_2}\nabla\rho_2^{n+1/2}\delta_t\nabla\rho_2^{n+1/2} + \kappa_{\rho_1\rho_2}(\nabla\rho_1^{n+1/2}\delta_t\nabla\rho_2^{n+1/2} + \nabla\rho_2^{n+1/2}\delta_t\nabla\rho_1^{n+1/2}) + \\
&\alpha_1\rho_1\delta_t\rho_1 + \alpha_2\rho_2\delta_t\rho_2]d\mathbf{x} \\
&= (\mathbf{u}^{n+1/2}, \delta_t\mathbf{u}^{n+1/2}) + (2q_1^{n+1/2}, \delta_t q_1^n) + (\mu_1^{n+1/2} - 2q_1^{n+1/2}\overline{\tfrac{\partial q_1}{\partial\rho_1}}^{n+1/2}, \delta_t\rho_1^{n+1/2}) + \\
&(\mu_2^{n+1/2} - 2q_1^{n+1/2}\overline{\tfrac{\partial q_1}{\partial\rho_2}}^{n+1/2}, \delta_t\rho_2^{n+1/2}) \\
&= (\mathbf{u}^{n+1/2}\delta_t\mathbf{u}^{n+1/2}) + [(2q_1^{n+1/2}, \delta_t q_1^{n+1/2}) - (2q_1^{n+1/2}\overline{\tfrac{\partial q_1}{\partial\rho_1}}^{n+1/2}, \delta_t\rho_1^{n+1/2}) - \\
&(2q_1^{n+1/2}\overline{\tfrac{\partial q_1}{\partial\rho_2}}^{n+1/2}, \delta_t\rho_2^{n+1/2})] + (\mu_1^{n+1/2}, \delta_t\rho_1^{n+1/2}) + (\mu_2^{n+1/2}, \delta_t\rho_2^{n+1/2}) \\
&= (\mathbf{u}^{n+1/2}\delta_t\mathbf{u}^{n+1/2}) + (\mu_1^{n+1/2}, \delta_t\rho_1^{n+1/2}) + (\mu_2^{n+1/2}, \delta_t\rho_2^{n+1/2}).
\end{aligned} \tag{5.24}$$

Taking the inner product of (5.19)-3 with $\mathbf{u}^{n+1/2}$, using identity (5.23), and performing integration by parts, we obtain

$$\begin{aligned}
&(\mathbf{u}^{n+1/2}, \delta_t\mathbf{u}^{n+1/2}) = -2(\tfrac{1}{Re_s}\mathbf{D}^{n+1/2} : \mathbf{D}^{n+1/2}) - (\tfrac{1}{Re_v}\nabla\cdot(\overline{\tfrac{1}{\sqrt{\rho}}}^{n+1/2}\mathbf{u}^{n+1/2}), \nabla\cdot(\overline{\tfrac{1}{\sqrt{\rho}}}^{n+1/2}\mathbf{u}^{n+1/2})) \\
&-(\mathbf{u}^{n+1/2}, \overline{\tfrac{1}{\sqrt{\rho}}}^{n+1/2}\overline{\rho_1}^{n+1/2}\nabla\mu_1^{n+1/2} + \overline{\tfrac{1}{\sqrt{\rho}}}^{n+1/2}\overline{\rho_2}^{n+1/2}\nabla\mu_2{}^{n+1/2})).
\end{aligned} \tag{5.25}$$

Taking the inner product of (5.19-1,2) with $\mu_1^{n+\frac{1}{2}}, \mu_2^{n+\frac{1}{2}}$, respectively, and performing integration by parts, we obtain

$$\begin{aligned}
&(\mu_1^{n+1/2}, \delta_t\rho_1^{n+1/2}) + (\mu_2^{n+1/2}, \delta_t\rho_2^{n+1/2}) = (\mathbf{u}^{n+1/2}, \overline{\tfrac{1}{\sqrt{\rho}}}^{n+1/2}\overline{\rho_1}^{n+1/2}\nabla\mu_1^{n+1/2} + \\
&\overline{\tfrac{1}{\sqrt{\rho}}}^{n+1/2}\overline{\rho_2}^{n+1/2}\nabla\mu_2{}^{n+1/2})) - (\nabla\mu_1^{n+1/2}, \nabla\mu_2^{n+1/2})\cdot\mathcal{M}\cdot(\nabla\mu_1^{n+1/2}, \nabla\mu_2^{n+1/2})^T.
\end{aligned} \tag{5.26}$$

Using (5.24), (5.25) and (5.26), we arrive at the conclusion

$$\begin{aligned}
&\tfrac{E^{n+1}-E^n}{\Delta t} = -2(\tfrac{1}{Re_s}\mathbf{D}^{n+1/2} : \mathbf{D}^{n+1/2}) - (\tfrac{1}{Re_v}\nabla\cdot(\overline{\tfrac{1}{\sqrt{\rho}}}^{n+1/2}\mathbf{u}^{n+1/2}), \nabla\cdot(\overline{\tfrac{1}{\sqrt{\rho}}}^{n+1/2}\mathbf{u}^{n+1/2})) \\
&-(\nabla\mu_1^{n+1/2}, \nabla\mu_2^{n+1/2})\cdot\mathcal{M}\cdot(\nabla\mu_1^{n+1/2}, \nabla\mu_2^{n+1/2})^T \le 0
\end{aligned} \tag{5.27}$$

provided $\mathcal{M} \ge 0$. □

5.3. Fully discrete numerical scheme

We discretize the semidiscrete equations in (5.19) using the second order finite difference discretization on staggered grids in space to obtain a fully discrete scheme as follows

Algorithm 2.

$$
\begin{cases}
\{\delta_t\rho_1^{n+1/2}+d_x(A_x(\overline{\rho}_1^{n+1/2}\overline{\frac{1}{\sqrt{\rho}}}^{n+1/2})u^{n+1/2})+d_y(A_y(\overline{\rho}_1^{n+1/2}\overline{\frac{1}{\sqrt{\rho}}}^{n+1/2})v^{n+1/2})= \\
M_1\Delta_h\mu_1^{n+1/2}-M_1\Delta_h\mu_2^{n+1/2}\}|_{i,j},\ i=1,\cdots,N_x,\ j=1,\cdots,N_y, \\
\{\delta_t\rho_2^{n+1/2}+d_x(A_x(\overline{\rho}_2^{n+1/2}\overline{\frac{1}{\sqrt{\rho}}}^{n+1/2})u^{n+1/2})+d_y(A_y(\overline{\rho}_2^{n+1/2}\overline{\frac{1}{\sqrt{\rho}}}^{n+1/2})v^{n+1/2})= \\
-M_1\Delta_h\mu_1^{n+1/2}+M_1\Delta_h\mu_2^{n+1/2}\}|_{i,j},\ i=1,\cdots,N_x,\ j=1,\cdots,N_y, \\
\{\delta_t u^{n+1/2}+\frac{1}{2}(\overline{u}^{n+1/2}D_x(\overline{\frac{1}{\sqrt{\rho}}}^{n+1/2}a_x u^{n+1/2})+A_x(\overline{\frac{1}{\sqrt{\rho}}}^{n+1/2}d_x(\overline{u}^{n+1/2}u^{n+1/2})) \\
+\frac{1}{2}(a_x(A_x\overline{v}^{n+1/2}D_y(A_x(\overline{\frac{1}{\sqrt{\rho}}}^{n+1/2})u^{n+1/2}))+A_x(\overline{\frac{1}{\sqrt{\rho}}}^{n+1/2})d_y(A_y u^{n+1/2}A_x(\overline{v}^{n+1/2})) \\
=g_{v1}\}|_{i+\frac{1}{2},j},\ i=1,\cdots,N_x-1,\ j=1,\cdots,N_y, \\
\{\delta_t v^{n+1/2}+\frac{1}{2}(a_x(A_y\overline{u}^{n+1/2}D_x(A_y(\overline{\frac{1}{\sqrt{\rho}}}^{n+1/2})v^{n+1/2})) \\
+A_y(\overline{\frac{1}{\sqrt{\rho}}}^{n+1/2})d_x(A_y\overline{u}^{n+1/2}A_x v^{n+1/2})) \\
+\frac{1}{2}(\overline{v}^{n+1/2}D_y(\overline{\frac{1}{\sqrt{\rho}}}^{n+1/2}a_y v^{n+1/2})+A_y(\overline{\frac{1}{\sqrt{\rho}}}^{n+1/2}d_y(\overline{v}^{n+1/2}v^{n+1/2})))=g_{v2}\}|_{i,j+\frac{1}{2}}, \\
i=1,\cdots,N_x,\ j=1,\cdots,N_y-1, \\
\{\delta_t q_1^{n+1/2}=\overline{\frac{\partial q_1}{\partial\rho_1}}^{n+1/2}\delta_t\rho_1^{n+1/2}+\overline{\frac{\partial q_1}{\partial\rho_2}}^{n+1/2}\delta_t\rho_2^{n+1/2}\}|_{i,j},\ i=1,\cdots,N_x,\ j=1,\cdots,N_y,
\end{cases}
\tag{5.28}
$$

where

$$
\begin{aligned}
g_{v1}&=A_x(\overline{\frac{1}{\sqrt{\rho}}}^{n+1/2})(2D_x(\frac{1}{Re_s^{n+1/2}}d_x(A_x(\overline{\frac{1}{\sqrt{\rho}}}^{n+1/2})u^{n+1/2})) \\
&+d_y(A_x(A_y\frac{1}{Re_s^{n+1/2}})D_y(A_x(\overline{\frac{1}{\sqrt{\rho}}}^{n+1/2})u^{n+1/2}))) \\
&+A_x(\overline{\frac{1}{\sqrt{\rho}}}^{n+1/2})d_y(A_x(A_y\frac{1}{Re_s^{n+1/2}})D_x(A_y(\overline{\frac{1}{\sqrt{\rho}}}^{n+1/2})v^{n+1/2})) \\
&+A_x(\overline{\frac{1}{\sqrt{\rho}}}^{n+1/2})D_x(\frac{1}{Re_v^{n+1/2}}d_x(A_x(\overline{\frac{1}{\sqrt{\rho}}}^{n+1/2})u^{n+1/2})) \\
&+A_x(\overline{\frac{1}{\sqrt{\rho}}}^{n+1/2})D_x(\frac{1}{Re_v^{n+1/2}}d_y(A_y(\overline{\frac{1}{\sqrt{\rho}}}^{n+1/2})v^{n+1/2})) \\
&-A_x(\overline{\rho_1}^{n+1/2}\overline{\frac{1}{\sqrt{\rho}}}^{n+1/2})D_x(\mu_1^{n+1/2})-A_x(\overline{\rho_2}^{n+1/2}\overline{\frac{1}{\sqrt{\rho}}}^{n+1/2})D_x(\mu_2^{n+1/2}), \\
g_{v2}&=A_y(\overline{\frac{1}{\sqrt{\rho}}}^{n+1/2})(d_x(A_x(A_y\frac{1}{Re_s^{n+1/2}})D_x(A_y(\overline{\frac{1}{\sqrt{\rho}}}^{n+1/2})v^{n+1/2})) \\
&+2D_y(\frac{1}{Re_s^{n+1/2}}d_y(A_y(\overline{\frac{1}{\sqrt{\rho}}}^{n+1/2})v^{n+1/2}))) \\
&+A_y(\overline{\frac{1}{\sqrt{\rho}}}^{n+1/2})d_x(A_x(A_y\frac{1}{Re_s^{n+1/2}})D_y(A_x(\overline{\frac{1}{\sqrt{\rho}}}^{n+1/2})u^{n+1/2})) \\
&+A_y(\overline{\frac{1}{\sqrt{\rho}}}^{n+1/2})D_y(\frac{1}{Re_v^{n+1/2}}d_x(A_x(\frac{1}{\sqrt{\rho}})u^{n+1/2})) \\
&+A_y(\overline{\frac{1}{\sqrt{\rho}}}^{n+1/2})D_y(\frac{1}{Re_v^{n+1/2}}d_y(A_y(\overline{\frac{1}{\sqrt{\rho}}}^{n+1/2})v^{n+1/2})) \\
&-A_y(\overline{\rho_1}^{n+1/2}\overline{\frac{1}{\sqrt{\rho}}}^{n+1/2})D_y(\mu_1^{n+1/2})-A_y(\overline{\rho_2}^{n+1/2}\overline{\frac{1}{\sqrt{\rho}}}^{n+1/2})D_y(\mu_2^{n+1/2}).
\end{aligned}
\tag{5.29, 5.30}
$$

For any time step t_n, $\rho_i^n, \mu_i^n, i=1,2$ satisfy discrete homogeneous Neumann boundary conditions (5.8) and u^n, v^n satisfy the discrete homogeneous Dirichlet boundary conditions (5.9). The discrete Reynolds numbers are defined as follows

$$\begin{aligned}
&\{\frac{1}{Re_s^{n+1/2}} = \overline{(\frac{\rho_1}{\rho})}^{n+1/2}\frac{1}{Re_{s1}} + \overline{(\frac{\rho_2}{\rho})}^{n+1/2}\frac{1}{Re_{s2}}\}|_{i,j}, i = 1, \cdots, N_x, j = 1, \cdots, N_y,\\
&\{\frac{1}{Re_v^{n+1/2}} = \overline{(\frac{\rho_1}{\rho})}^{n+1/2}\frac{1}{Re_{v1}} + \overline{(\frac{\rho_2}{\rho})}^{n+1/2}\frac{1}{Re_{v2}}\}|_{i,j}, i = 1, \cdots, N_x, j = 1, \cdots, N_y.
\end{aligned} \tag{5.31}$$

Theorem 5.2. *Scheme (5.28) is unconditionally energy stable, and the discrete total energy satisfies the following identity*

$$\begin{aligned}
&\frac{E_h^{n+1}-E_h^n}{\Delta t} = -2(\frac{1}{Re_s}, \mathbf{D}_h^{n+1/2} : \mathbf{D}_h^{n+1/2})_2 - (\frac{1}{Re_v}tr(\mathbf{D}_h^{n+1/2}), tr(\mathbf{D}_h^{n+1/2}))_2\\
&-M_1(\nabla(\mu_1^{n+1/2} - \mu_2^{n+1/2}), \nabla(\mu_1^{n+1/2} - \mu_2^{n+1/2}))_2 \le 0,
\end{aligned} \tag{5.32}$$

where the discrete total energy is defined by

$$\begin{aligned}
&E_h^n = \tfrac{1}{2}[u^n, u^n]_{ew} + \tfrac{1}{2}[v^n, v^n]_{ns} + (q_1^n, q_1^n)_2 + \tfrac{\alpha_1}{2}(\rho_1^n, \rho_1^n)_2 + \tfrac{\alpha_2}{2}(\rho_2^n, \rho_2^n)_2 - (A, 1)_2\\
&+\tfrac{1}{2}\kappa_{\rho_1\rho_1}(\nabla\rho_1^n, \nabla\rho_1^n)_h + \tfrac{1}{2}\kappa_{\rho_2\rho_2}(\nabla\rho_2^n, \nabla\rho_2^n)_h + \kappa_{\rho_1\rho_2}(\nabla\rho_1^n, \nabla\rho_2^n)_h,
\end{aligned} \tag{5.33}$$

and

$$\mathbf{D}_h^{n+1/2} = \begin{pmatrix} d_x(A_x(\overline{\frac{1}{\sqrt{\rho}}}^{n+1/2})u^{n+1/2})) & \frac{1}{2}S \\ \frac{1}{2}S & d_y(A_y(\overline{\frac{1}{\sqrt{\rho}}}^{n+1/2})v^{n+1/2})) \end{pmatrix} \tag{5.34}$$

where $S = D_x(A_y(\overline{\frac{1}{\sqrt{\rho}}}^{n+1/2})v^{n+1/2}) + D_y(A_x(\overline{\frac{1}{\sqrt{\rho}}}^{n+1/2})u^{n+1/2}))$.

Remark 5.3. We note that using Lemmas 5.1–5.3, we obtain the following identities

$$\begin{aligned}
&(u^{n+1/2}, \tfrac{1}{2}(a_x(A_y\overline{u}^{n+1/2}D_x(A_y(\overline{\frac{1}{\sqrt{\rho}}}^{n+1/2})v^{n+1/2})) + A_y(\overline{\frac{1}{\sqrt{\rho}}}^{n+1/2})d_x(A_y\overline{u}^{n+1/2}A_xv^{n+1/2}))\\
&+\tfrac{1}{2}(\overline{v}^{n+1/2}D_y(\overline{\frac{1}{\sqrt{\rho}}}^{n+1/2}a_yv^{n+1/2}) + A_y(\overline{\frac{1}{\sqrt{\rho}}}^{n+1/2}d_y(\overline{v}^{n+1/2}v^{n+1/2})))) = 0,\\
&(v^{n+1/2}, \tfrac{1}{2}(a_x(A_y\overline{u}^{n+1/2}D_x(A_y(\overline{\frac{1}{\sqrt{\rho}}}^{n+1/2})v^{n+1/2})) + A_y(\overline{\frac{1}{\sqrt{\rho}}}^{n+1/2})d_x(A_y\overline{u}^{n+1/2}A_xv^{n+1/2}))\\
&+\tfrac{1}{2}(\overline{v}^{n+1/2}D_y(\overline{\frac{1}{\sqrt{\rho}}}^{n+1/2}a_yv^{n+1/2}) + A_y(\overline{\frac{1}{\sqrt{\rho}}}^{n+1/2}d_y(\overline{v}^{n+1/2}v^{n+1/2})))) = 0.
\end{aligned} \tag{5.35}$$

Proof. It follows from the definition of E_h^n that

$$\begin{aligned}
&\frac{E_h^{n+1}-E_h^n}{\Delta t} = [\tfrac{u^{n+1}+u^n}{2}, \tfrac{u^{n+1}-u^n}{\Delta t}]_{ew} + [\tfrac{v^{n+1}+v^n}{2}, \tfrac{v^{n+1}-v^n}{\Delta t}]_{ns} + 2(\tfrac{q_1^{n+1}+q_1^n}{2}, \tfrac{q_1^{n+1}-q_1^n}{\Delta t})_2\\
&+\alpha_1(\tfrac{\rho_1^{n+1}+\rho_1^n}{2}, \tfrac{\rho_1^{n+1}-\rho_1^n}{\Delta t})_2 + \alpha_2(\tfrac{\rho_2^{n+1}+\rho_2^n}{2}, \tfrac{\rho_2^{n+1}-\rho_2^n}{\Delta t})_2\\
&+\kappa_{\rho_1\rho_1}(\tfrac{\nabla\rho_1^{n+1}+\nabla\rho_1^n}{2}, \tfrac{\nabla\rho_1^{n+1}-\nabla\rho_1^n}{\Delta t})_h + \kappa_{\rho_2\rho_2}(\tfrac{\nabla\rho_2^{n+1}+\nabla\rho_2^n}{2}, \tfrac{\nabla\rho_2^{n+1}-\nabla\rho_2^n}{\Delta t})_h\\
&+\kappa_{\rho_1\rho_2}[(\tfrac{\nabla\rho_1^{n+1}+\nabla\rho_1^n}{2}, \tfrac{\nabla\rho_2^{n+1}-\nabla\rho_2^n}{\Delta t})_h + (\tfrac{\nabla\rho_2^{n+1}+\nabla\rho_2^n}{2}, \tfrac{\nabla\rho_1^{n+1}-\nabla\rho_1^n}{\Delta t})_h]\\
&= [\tfrac{u^{n+1}+u^n}{2}, \tfrac{u^{n+1}-u^n}{\Delta t}]_{ew} + [\tfrac{v^{n+1}+v^n}{2}, \tfrac{v^{n+1}-v^n}{\Delta t}]_{ns} + (\mu_1^{n+1/2}, \tfrac{\rho_1^{n+1}-\rho_1^n}{\Delta t})_2 + (\mu_2^{n+1/2}, \tfrac{\rho_2^{n+1}-\rho_2^n}{\Delta t})_2.
\end{aligned} \tag{5.36}$$

Taking the inner product of (5.28-3,4) with $u^{n+1/2}$, $v^{n+1/2}$ respectively and using identify (5.35), we obtain

$$\begin{aligned}
&[\tfrac{u^{n+1}+u^n}{2}, \tfrac{u^{n+1}-u^n}{\Delta t}]_{ew} + [\tfrac{v^{n+1}+v^n}{2}, \tfrac{v^{n+1}-v^n}{\Delta t}]_{ns}\\
&= -2(\tfrac{1}{Re_s}, \mathbf{D}_h^{n+1/2} : \mathbf{D}_h^{n+1/2})_2 - (\tfrac{1}{Re_v}tr(\mathbf{D}_h^{n+1/2}), tr(\mathbf{D}_h^{n+1/2}))_2\\
&-[u^{n+1/2}, A_x(\overline{\rho_1}^{n+1/2}\overline{\tfrac{1}{\sqrt{\rho}}}^{n+1/2})D_x(\mu_1^{n+1/2}) + A_x(\overline{\rho_2}^{n+1/2}\overline{\tfrac{1}{\sqrt{\rho}}}^{n+1/2})D_x(\mu_2^{n+1/2})]_{ew}\\
&-[v^{n+1/2}, A_y(\overline{\rho_1}^{n+1/2}\overline{\tfrac{1}{\sqrt{\rho}}}^{n+1/2})D_y(\mu_1^{n+1/2}) + A_y(\overline{\rho_2}^{n+1/2}\overline{\tfrac{1}{\sqrt{\rho}}}^{n+1/2})D_y(\mu_2^{n+1/2})]_{ns},
\end{aligned} \tag{5.37}$$

where we have used Lemmas 5.1 and 5.3. Taking the inner product of (5.28-1,2) with $\mu_1^{n+1/2}, \mu_2^{n+1/2}$, respectively, and performing "summation-by-parts", we obtain

$$(\mu_1^{n+1/2}, \tfrac{\rho_1^{n+1/2}-\rho_1^n}{\Delta t})_2 + (\mu_2^{n+1}, \tfrac{\rho_2^{n+1}-\rho_2^n}{\Delta t})_2 = [u^{n+1/2}, A_x(\overline{\rho_1}^{n+1/2}\overline{\tfrac{1}{\sqrt{\rho}}}^{n+1/2})D_x(\mu_1^{n+1/2}) +$$
$$A_x(\overline{\rho_2}^{n+1/2}\overline{\tfrac{1}{\sqrt{\rho}}}^{n+1/2})D_x(\mu_2^{n+1/2})]_{ew} + [v^{n+1/2}, A_y(\overline{\rho_1}^{n+1/2}\overline{\tfrac{1}{\sqrt{\rho}}}^{n+1/2})D_y(\mu_1^{n+1/2}) + \tag{5.38}$$
$$A_y(\overline{\rho_2}^{n+1/2}\overline{\tfrac{1}{\sqrt{\rho}}}^{n+1/2})D_y(\mu_2^{n+1/2})]_{ns} - (\nabla(\mu_1^{n+1/2}-\mu_2^{n+1/2}), -M_1\nabla(\mu_1^{n+1/2}-\mu_2^{n+1/2})),$$

where we have used Lemma 5.1. Combining (5.36), (5.37) and (5.38), we obtain

$$\begin{aligned}&\tfrac{E_h^{n+1}-E_h^n}{\Delta t} = -2(\tfrac{1}{Re_s}, \mathbf{D}_h^{n+1/2} : \mathbf{D}_h^{n+1/2})_2 - (\tfrac{1}{Re_v} tr(\mathbf{D}_h^{n+1/2}), tr(\mathbf{D}_h^{n+1/2}))_2 \\ &-M_1(\nabla(\mu_1^{n+1/2}-\mu_2^{n+1/2}), \nabla(\mu_1^{n+1/2}-\mu_2^{n+1/2}))_2 \le 0,\end{aligned} \tag{5.39}$$

provided $M_1 \ge 0$. Having established unconditional energy stability, we now turn to the solvability issue of the linear system of equations. □

5.4. Unique solvability of the resulting linear system from the fully discrete scheme

We denote the linear system resulting from the fully discrete numerical scheme (5.28) as follows

$$\mathcal{A}\cdot\mathbf{X} = \mathcal{G}, \tag{5.40}$$

where the coefficient matrix $\mathcal{A}$ is given in (A.6) in Appendix, $\mathbf{X} = (\mu_1, \mu_2, u, v, q_1, \rho_1, \rho_2)$ is the unknown of the linear system, whose superscripts $n+1$ are removed for simplicity, and $\mathcal{G} = (g_1, g_2, g_3, g_4, g_5, g_6, g_7)^T$ denotes all the right hand side terms at the nth time step, where the superscripts n are removed for simplicity as well. Notice that each entry in $\mathbf{X}$ and $\mathcal{G}$ is a large vector itself. The corresponding homogeneous system is given by

$$\mathcal{A}\cdot\mathbf{X} = 0. \tag{5.41}$$

Theorem 5.3. *Linear system (5.40) admits a unique solution.*

Proof. To prove the well-posedness of the system (5.40), it suffices to prove that the corresponding homogeneous system (5.41) admits only the zero solution. Let $\mathbf{X} = (\mu_1, \mu_2, u, v, q_1, \rho_1, \rho_2)$ be a solution of $\mathcal{A}\cdot\mathbf{X} = 0$. We form the inner product of the left hand side with $\mathbf{X}$ to obtain

$$\begin{aligned}0 &= (\mathcal{A}\cdot\mathbf{X}, \mathbf{X})_2 = (M_1\nabla(\mu_1-\mu_2), \nabla(\mu_1-\mu_2))_2 + \tfrac{2}{\Delta t}[u,u]_{ew} + \tfrac{2}{\Delta t}[v,v]_{ns} + \tfrac{4}{\Delta t}(q_1,q_1)_2 \\ &+2(\tfrac{1}{Re_s}, \mathbf{D}_h : \mathbf{D}_h)_2 + (\tfrac{1}{Re_v} tr(\mathbf{D}_h), tr(\mathbf{D}_h))_2 + \tfrac{2}{\Delta t}[\kappa_{\rho_1\rho_1}(\nabla\rho_1, \nabla\rho_1)_h + \kappa_{\rho_2\rho_2}(\nabla\rho_2, \nabla\rho_2)_h] \\ &+\tfrac{4}{\Delta t}\kappa_{\rho_1\rho_2}(\nabla\rho_1, \nabla\rho_2)_h + \tfrac{2\alpha_1}{\Delta t}(\rho_1,\rho_1)_2 + \tfrac{2\alpha_2}{\Delta t}(\rho_2,\rho_2)_2 \\ &\ge C((\nabla\rho_1, \nabla\rho_1)_h + (\nabla\rho_2, \nabla\rho_2)_h + [u,u]_{ew} + [v,v]_{ns} + \|q_1\|_{l_2}^2) + \tfrac{2\alpha_1}{\Delta t}(\rho_1,\rho_1)_2 + \tfrac{2\alpha_2}{\Delta t}(\rho_2,\rho_2)_2,\end{aligned} \tag{5.42}$$

where we have used $\mathbf{K} > 0$, C is a positive constant and $\mathbf{D}_h$ is defined in (A.2). In the case of $\alpha_1 = \alpha_2 = 0$, the above inequality implies

$$D_x\rho_1 = D_y\rho_1 = 0, \quad D_x\rho_1 = D_y\rho_2 = 0, \quad u = v = 0, \quad q_1 = 0. \tag{5.43}$$

In the last two equations of the homogeneous system in (A.9), using $D_x\rho_1 = D_y\rho_1 = 0$, $D_x\rho_1 = D_y\rho_2 = 0$ and $q_1 = 0$, we obtain

$$\mu_1 = \mu_2 = 0. \tag{5.44}$$
$$\rho_1 = \rho_2 = 0 \tag{5.45}$$

follows from the first two equations of the homogeneous system (A.9) after substituting $u = v = 0$ and $\mu_1 = \mu_2 = 0$. So, $\mathbf{X} = \mathbf{0}$. Thus, linear system (5.40) admits a unique solution.

In the case of $\alpha_1 > 0, \alpha_2 > 0$, the inequality implies directly

$$\rho_1 = \rho_2 = q_1 = 0. \tag{5.46}$$

It implies $\mu_1 = \mu_2 = 0$. Once again, the only solution is the zero solution of the homogeneous system. □

Remark 5.4. A second order, energy stable BDF scheme can be developed as well, which will not be presented in this paper.

6. Numerical results and discussions

6.1. Accuracy test

We conduct a mesh refinement test to verify the convergence rate of the numerical scheme by considering (3.2) with a double-well bulk free energy

$$h(\rho_1, \rho_2, T) = \rho_1^2(\rho_1 - 1)^2 + \rho_2^2(\rho_2 - 1)^2, \tag{6.1}$$

in a rectangular domain $\Omega = [0, 1] \times [0, 1]$. We add forcing terms to the equation system such that it admits the following exact solution:

$$\begin{aligned} &\rho_1(x, y, t = 0) = 1 + 0.1cos(\pi x)cos(\pi y)e^{-t}, \\ &\rho_2(x, y, t = 0) = 1 + 0.1cos(2\pi x)cos(2\pi y)e^{-t}, \\ &\mathbf{v} = (0.1sin(\pi x)sin(\pi y)e^{-t}, \quad 0.1sin(\pi x)sin(\pi y)e^{-t}). \end{aligned} \tag{6.2}$$

We set $N_x = N_y = N$, and the time step as Δt. To test the convergence rate in time, we first fix $N = 256$ and change the time step from 4×10^{-3} to 0.125×10^{-3} to calculate the l_∞ norm of the difference between the numerical solutions with consecutive grid sizes at $T = 0.1$, i.e. $\|(\cdot)^{\Delta t}(T) - (\cdot)^{2\Delta t}(T)\|_\infty$. Then, we fix time step $\Delta t = 10^{-4}$, vary the spatial grid number from 8 to 256 and calculate the l_∞ norm of the difference between the numerical solutions with consecutive grid sizes at $T = 0.1$, i.e. $\|(\cdot)^h(T) - (\cdot)^{2h}(T)\|_\infty$. In both space and time, we calculate the convergence rate using $p = log_2\left(\frac{\|(\cdot)^{2h}(T) - (\cdot)^{4h}(T)\|_\infty}{\|(\cdot)^h(T) - (\cdot)^{2h}(T)\|_\infty}\right)$, where h is the mesh size in time or space. The refinement results are tabulated in Table 6.1 and Table 6.2. For comparison, we also present the mesh refinement results in l_2 norm as well. We observe that the proposed scheme is indeed second-order accurate in both time and space for all variables.

6.2. Phase separation in binary compressible viscous fluids

To demonstrate stability and efficiency of the new scheme, we simulate phase separation dynamics using system (3.2) with the Flory-Huggins mixing energy

$$h(\rho_1, \rho_2, T) = \frac{k_B T}{m}\rho\left(\frac{1}{N_1}\frac{\rho_1}{\rho}ln\frac{\rho_1}{\rho} + \frac{1}{N_2}\frac{\rho_2}{\rho}ln\frac{\rho_2}{\rho} + \chi\frac{\rho_1\rho_2}{\rho^2}\right), \tag{6.3}$$

where we choose the characteristic scales so that $\frac{k_B T}{m} = 1$ in the simulation, N_1, N_2 are the polymerization indices and χ is the mixing coefficient, which are chosen respectively as in the simulation

$$N_1 = N_2 = 1, \qquad \chi = 2.5. \tag{6.4}$$

The plot of this energy density with the chosen parameter values as a function of $\frac{\rho_1}{\rho}$ is shown in Fig. 6.1-(a). The other dimensionless model parameters are chosen as follows

$$M_1 = 10^{-3}, \quad Re_s = 100, \quad Re_v = 300, \quad \kappa_{\rho_1\rho_1} = \kappa_{\rho_2\rho_2} = 4 \times 10^{-4}, \quad \kappa_{\rho_1\rho_2} = 0. \tag{6.5}$$

In order to identify the spinodal decomposition driving the phase separation in the binary polymer blends, we conduct a simple linear stability analysis on the hydrodynamic phase field model. We note that this compressible model admits a family of constant solutions:

$$\mathbf{v} = \mathbf{0}, \quad \rho_1 = \rho_1^0, \quad \rho_2 = \rho_2^0, \tag{6.6}$$

where ρ_1^0, ρ_2^0 are constants. We perturb the constant solutions with a normal mode as follows:

$$\mathbf{v} = \epsilon e^{\alpha t + i\mathbf{k}\cdot\mathbf{x}}\mathbf{v}^c, \quad \rho_1 = \rho_1^0 + \epsilon e^{\alpha t + i\mathbf{k}\cdot\mathbf{x}}{\rho_1}^c, \quad \rho_2 = \rho_2^0 + \epsilon e^{\alpha t + i\mathbf{k}\cdot\mathbf{x}}{\rho_2}^c, \tag{6.7}$$

where ϵ is a small parameter, representing the magnitude of the perturbation, and $\mathbf{v}^c, \rho_1^c, \rho_2^c$ are constants, α is the growth rate, and $\mathbf{k}$ is the wave number of the perturbation. Without loss of generality, we limit our study to 1 dimensional perturbation in $\mathbf{k}$ in the (x, y) plane. Substituting these perturbations into the equations in (3.2) and truncating the equations at order $O(\epsilon)$, we obtain the linearized equations. The dispersion equation of the linearized equation system of the compressible model [64] is given by an algebraic equation of α:

$$\begin{aligned} &(\eta^0 k^2 + \alpha\rho^0)\{\alpha^3\rho_0 + \alpha^2 k^2[\eta + \rho^0 M_1(h_{\rho_1\rho_1} + \kappa_{\rho_1\rho_1}k^2) + \rho^0 M_1(h_{\rho_2\rho_2} + \kappa_{\rho_2\rho_2}k^2)] \\ &-\alpha^2 k^2[2\rho^0 M_1(h_{\rho_1\rho_2} + \kappa_{\rho_1\rho_2}k^2)] + \alpha[\mathbf{p}^T\cdot\mathbf{C}\cdot\mathbf{p} + \mathbf{p}^T\cdot\mathbf{K}\cdot\mathbf{p}k^2]k^2 \\ &+\alpha\eta M_1[(h_{\rho_1\rho_1} + \kappa_{\rho_1\rho_1}k^2) + (h_{\rho_2\rho_2} + \kappa_{\rho_2\rho_2}k^2) - 2(h_{\rho_1\rho_2} + \kappa_{\rho_1\rho_2}k^2)]k^4 \\ &+k^4 M_1(\rho_1^0 + \rho_2^0)^2[(h_{\rho_1\rho_1} + \kappa_{\rho_1\rho_1}k^2)(h_{\rho_2\rho_2} + \kappa_{\rho_2\rho_2}k^2) - (h_{\rho_1\rho_2} + \kappa_{\rho_1\rho_2}k^2)^2]\} = 0, \end{aligned} \tag{6.8}$$

Table 6.1
Temporal refinement result for all variables. The model parameter values are chosen as $Re_s = 100$, $Re_v = 300$, $M_1 = 10^{-7}$, $\kappa_{\rho_1\rho_1} = \kappa_{\rho_2\rho_2} = 10^{-4}$, $\kappa_{\rho_1\rho_2} = \kappa_{\rho_2\rho_1} = 0$.

Δt	$\|{\rho_1}^{\Delta t} - {\rho_1}^{2\Delta t}\|_\infty$	Order	$\|{\rho_2}^{\Delta t} - {\rho_2}^{2\Delta t}\|_\infty$	Order	$\|\mathbf{u}^{\Delta t} - \mathbf{u}^{2\Delta t}\|_\infty$	Order
0.004						
0.002	0.4763×10^{-5}		0.4762×10^{-5}		0.4220×10^{-5}	
0.001	0.1183×10^{-5}	2.0100	0.1183×10^{-5}	2.0090	0.1042×10^{-5}	2.0179
0.0005	0.2948×10^{-6}	2.0047	0.2948×10^{-6}	2.0047	0.2591×10^{-6}	2.0080
0.00025	0.7333×10^{-7}	2.0072	0.7334×10^{-7}	2.0073	0.6460×10^{-7}	2.0080
0.000125	0.1829×10^{-7}	2.0034	0.1829×10^{-7}	2.0034	0.1613×10^{-7}	2.0010

Δt	$\|{\rho_1}^{\Delta t} - {\rho_1}^{2\Delta t}\|_2$	Order	$\|{\rho_2}^{\Delta t} - {\rho_2}^{2\Delta t}\|_2$	Order	$\|\mathbf{u}^{\Delta t} - \mathbf{u}^{2\Delta t}\|_2$	Order
0.004						
0.002	0.1911×10^{-5}		0.1930×10^{-5}		0.1571×10^{-5}	
0.001	0.4782×10^{-6}	1.9988	0.4829×10^{-6}	1.9991	0.3895×10^{-6}	2.0121
0.0005	0.1196×10^{-6}	1.9992	0.1207×10^{-6}	1.9995	0.9707×10^{-7}	2.0049
0.00025	0.2989×10^{-7}	2.0005	0.3017×10^{-7}	2.0008	0.2422×10^{-7}	2.0023
0.000125	0.7475×10^{-8}	1.9998	0.7546×10^{-8}	1.9996	0.6054×10^{-8}	2.0007

Table 6.2
Spatial refinement result for all variables. The model parameter values are chosen as $Re_s = 1$, $Re_v = 3$, $M_1 = 10^{-4}$, $\kappa_{\rho_1\rho_1} = \kappa_{\rho_2\rho_2} = 10^{-4}$, $\kappa_{\rho_1\rho_2} = \kappa_{\rho_2\rho_1} = 0$.

N	$\|{\rho_1}^h - {\rho_1}^{2h}\|_\infty$	Order	$\|{\rho_2}^h - {\rho_2}^{2h}\|_\infty$	Order	$\|\mathbf{u}^h - \mathbf{u}^{2h}\|_\infty$	Order
4						
8	0.5997×10^{-3}		0.2182×10^{-2}		0.3790×10^{-2}	
16	0.2463×10^{-3}	1.2836	0.4933×10^{-3}	2.1454	0.1133×10^{-2}	2.0168
32	0.6697×10^{-4}	1.8792	0.1043×10^{-3}	2.2407	0.2877×10^{-3}	1.9779
64	0.1664×10^{-4}	2.0084	0.2464×10^{-4}	2.0826	0.7288×10^{-4}	1.9814
128	0.4160×10^{-5}	2.0003	0.6088×10^{-5}	2.0168	0.1828×10^{-4}	1.9946

N	$\|{\rho_1}^h - {\rho_1}^{2h}\|_2$	Order	$\|{\rho_2}^h - {\rho_2}^{2h}\|_2$	Order	$\|\mathbf{u}^h - \mathbf{u}^{2h}\|_2$	Order
4						
8	0.3115×10^{-3}		0.1160×10^{-2}		0.2105×10^{-2}	
16	0.8228×10^{-4}	1.9210	0.1605×10^{-3}	2.8536	0.5237×10^{-3}	2.0071
32	0.1894×10^{-4}	2.1186	0.3081×10^{-4}	2.3814	0.1309×10^{-3}	1.9994
64	0.4626×10^{-5}	2.0340	0.7136×10^{-5}	2.1102	0.3284×10^{-4}	1.9958
128	0.1151×10^{-5}	2.0065	0.1747×10^{-5}	2.0299	0.8259×10^{-5}	1.9916

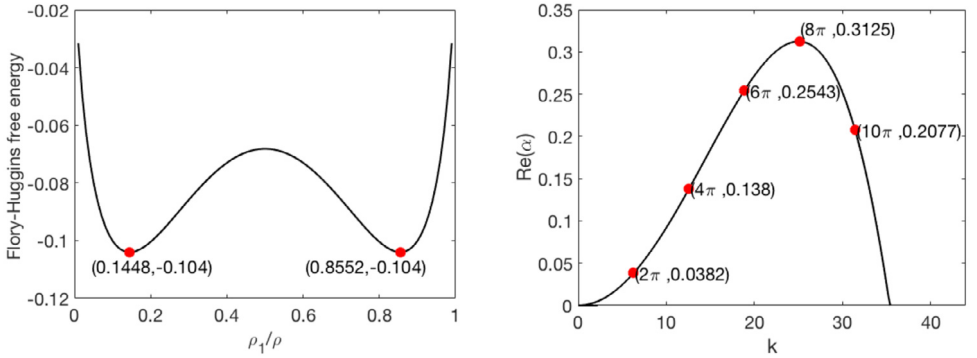

(a) Flory-Huggins mixing energy density function with respect to $\frac{\rho_1}{\rho}$

(b) Unstable mode

Fig. 6.1. (a) Flory-Huggins mixing energy density function with respect to the mass density fraction $\frac{\rho_1}{\rho}$ at the chosen parameter values. The two minima are labeled by dots in the curve. (b) The unstable mode with parameter values: $N_1 = N_2 = 1$, $\chi = 2.5$, $M_1 = 10^{-3}$, $Re_s = 100$, $Re_v = 300$, $\kappa_{\rho_1\rho_1} = \kappa_{\rho_2\rho_2} = 0.0004$, $\kappa_{\rho_1\rho_2} = 0$.

where $\eta = 2\eta^0 + \overline{\eta}^0$, $\mathbf{p} = (\rho_1^0, \rho_2^0)^T$ is the steady state solution of the system. In the following, we set $\rho_1^0 = \rho_2^0 = 0.5$. $\mathbf{K}$ is the coefficient matrix of the conformational entropy and $\mathbf{C}$ is the Hessian of bulk energy $h(\rho_1, \rho_2, T)$ with respect to ρ_1 and ρ_2,

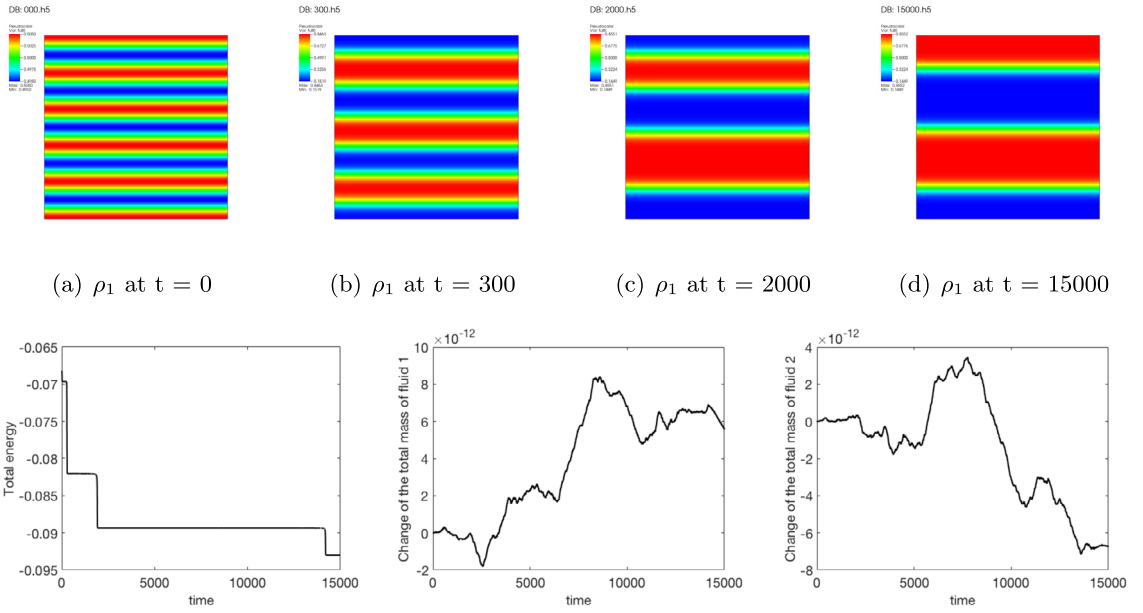

(a) ρ_1 at t = 0 (b) ρ_1 at t = 300 (c) ρ_1 at t = 2000 (d) ρ_1 at t = 15000

(e) Total Energy (f) Difference of total mass of the component 1 with its initial total mass (g) Difference of total mass of the component 2 with its initial total mass

Fig. 6.2. (a-d) Snapshots of ρ_1 at different times as a solution of system (3.2) with the Flory-Huggins mixing energy (6.3) without hydrodynamics. (e) The total energy (5.33) of system (3.2). Two major coarsening events bring the phase of the binary system into the final state shown in (d). ρ_2 is given by $1-\rho_1$. The total mass of both phases are conserved as shown in (f-g).

$$\mathbf{K}=\begin{pmatrix}\kappa_{\rho_1\rho_1} & \kappa_{\rho_1\rho_2}\\ \kappa_{\rho_1\rho_2} & \kappa_{\rho_2\rho_2}\end{pmatrix}, \mathbf{C}=\begin{pmatrix}h_{\rho_1\rho_1} & h_{\rho_1\rho_2}\\ h_{\rho_1\rho_2} & h_{\rho_2\rho_2}\end{pmatrix}. \tag{6.9}$$

Obviously, $\alpha=-\frac{\eta^0}{\rho^0}k^2<0$ is a solution of the dispersion equation (6.8), which contributes a stable mode. Since we can not get the closed forms of the solutions, we use numerical calculations to investigate the potential unstable modes in this model. Based on the model parameters listed above, we obtain only one unstable mode, shown in Fig. 6.1-(b). This unstable mode is dominated by the mixing energy, independent of hydrodynamics, in the model. Next, we will numerically simulate phase separation phenomena due to the unstable perturbation on the constant steady state without and with hydrodynamics, respectively.

6.2.1. Phase separation without hydrodynamics

Based on unstable mode shown in Fig. 6.1-b, we add a 1D perturbation with wave number $k=10\pi$ to the steady state and observe its ensuing nonlinear dynamics. Since the eigenvector corresponding to the unstable mode shown in Fig. 6.1-b is $(\rho_1^c,\rho_2^c)=(1,-1)$, we impose the initial conditions specifically as follows

$$\rho_1(x,y,t=0)=0.5+0.005\times cos(10\pi y),\qquad \rho_2(x,y,t=0)=0.5-0.005\times cos(10\pi y). \tag{6.10}$$

Since $\rho_1+\rho_2=1$ in the thermodynamic model without hydrodynamics, we show the phase behavior of ρ_1 only. The time evolution of ρ_1 at a few selected times are shown in Fig. 6.2. Firstly, we observe that the growth rate of the numerical solutions ρ_1 near the equilibrium state is $\alpha=0.2077$, which matches with linear stability analysis result shown in Fig. 6.1-b. In the long-time behavior, we observe that ρ_1 develops small-scale structures and then coarsens to large-scale structures eventually. In Fig. 6.2, we show numerical solutions at several time slots and the corresponding total energy up to $t=15000$. The system goes through three coarsening events which are captured by the phase morphology at different times shown in the Fig. 6.2(a-d), leading to a four-band structure.

6.2.2. Phase separation with hydrodynamics

When hydrodynamics is coupled with the thermodynamical phase evolution, its role must show up somewhere. Here, we would like to investigate how hydrodynamic will impact on phase separation dynamics. Since the eigenvector corresponding to the unstable mode shown in Fig. 6.1-b is $(\rho_1^c,\rho_2^c)=(1,-1,0)$, we adopt the same initial conditions for ρ_1 and ρ_2 as before and a zero velocity condition:

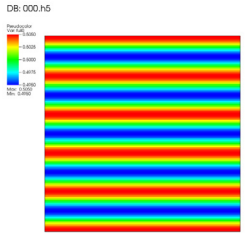

(a) ρ_1 at t = 0

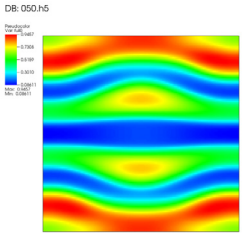

(b) ρ_1 at t = 50

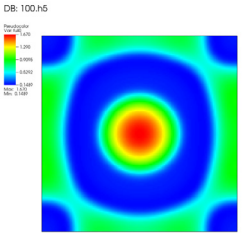

(c) ρ_1 at t = 100

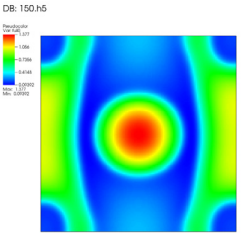

(d) ρ_1 at t = 150

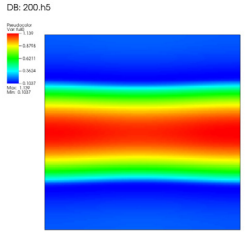

(e) ρ_1 at t = 200

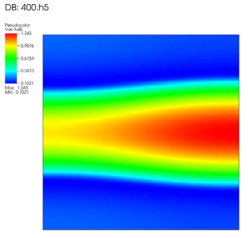

(f) ρ_1 at t = 400

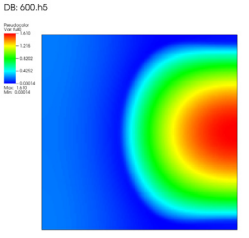

(g) ρ_1 at t = 600

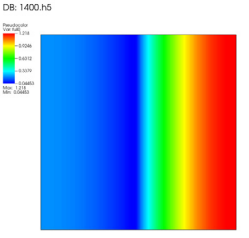

(h) ρ_1 at t = 1400

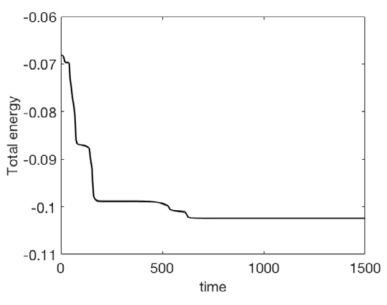

(i) Total Energy

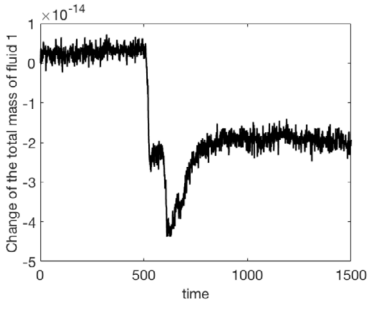

(j) Difference of total mass of the component 1 with its initial total mass

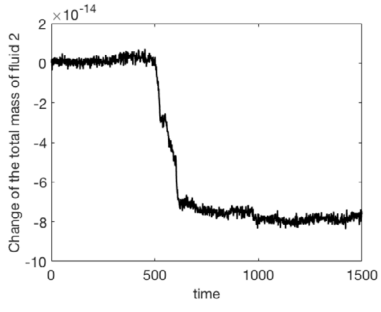

(k) Difference of total mass of the component 2 with its initial total mass

Fig. 6.3. (a-h) Snapshots of ρ_1 at different times as a solution of system (3.2) with the Flory-Huggins mixing energy (6.3) and hydrodynamic interaction. (i) Total energy (5.33) of system (3.2) with the Flory-Huggins mixing energy (6.3); (j, k) Difference of the total mass of component 1 and 2 compared with the initial mass, indicating mass conservation of both phases in the simulation. The path of phase separation dynamics and the final phase morphology differ drastically from those without hydrodynamics.

$$\begin{aligned} &\rho_1(x, y, 0) = 0.5 + 0.005 \times cos(10\pi\, y), \qquad \rho_2(x, y, 0) = 0.5 - 0.005 \times cos(10\pi\, y), \\ &\mathbf{v}(x, y, 0) = (0, 0). \end{aligned} \tag{6.11}$$

When hydrodynamics is considered, the local total mass density ρ is no longer spatially homogeneous anymore. However, phase separation goes on as shown in Fig. 6.3 and Fig. 6.4. In Fig. 6.3, we observe that the total energy of the system is dissipative and the total mass of component 1 and 2 are conserved in the domain globally. The velocity field in the domain is plotted at the selected times. Vorticities form and disperse eventually as the phase morphology approaches a steady state. The induced nontrivial velocity field promotes the transport of materials across the domain leading to a two-band phase morphology, which is a global energy stable state. In contrast, the final phase morphology developed in the phase separation without hydrodynamics is only a local energy stable state, which can be explained by the comparison of the total energy evolutions shown in Fig. 6.2-e and Fig. 6.3-i, respectively. This tells us that hydrodynamics indeed changes local densities, the path of phase evolution and even the final energy steady states of fluid mixtures. This is alarming, indicating that hydrodynamic effects are instrumental in determining the correct spatial phase diagram for the binary fluid mixture.

Fig. 6.5-(a) depicts the total free energy of the phase separation without hydrodynamics calculated using the original formula

$$\begin{aligned} &E_h^n = (h(\rho_1^n, \rho_2^n, T), 1)_2 \\ &+\tfrac{1}{2}\kappa_{\rho_1\rho_1}(\nabla\rho_1^n, \nabla\rho_1^n)_h + \tfrac{1}{2}\kappa_{\rho_2\rho_2}(\nabla\rho_2^n, \nabla\rho_2^n)_h + \kappa_{\rho_1\rho_2}(\nabla\rho_1^n, \nabla\rho_2^n)_h, \end{aligned} \tag{6.12}$$

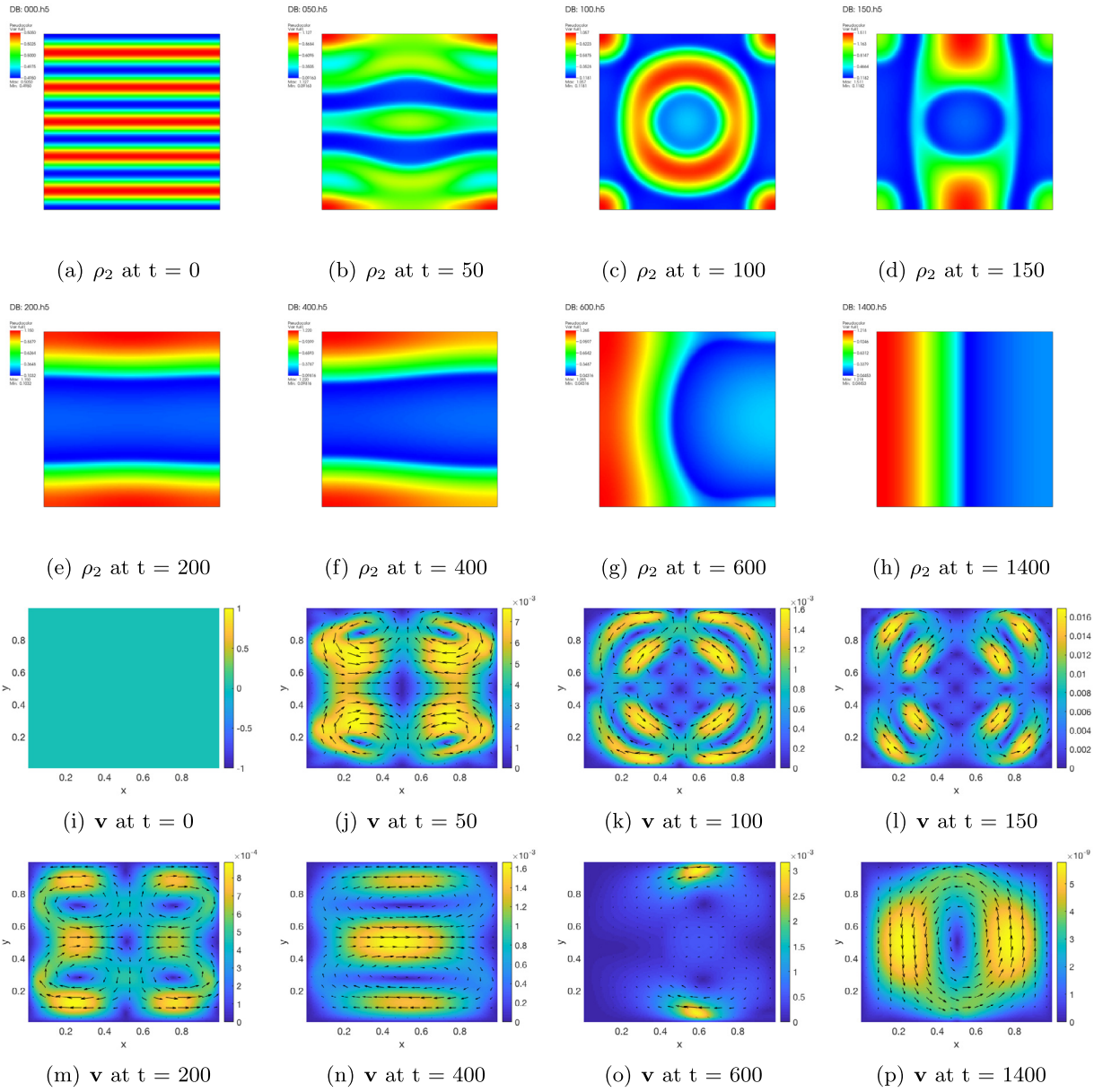

Fig. 6.4. (a-h) Snapshots of ρ_2 at different times as a solution of system (3.2) with the Flory-Huggins mixing energy (6.3) and hydrodynamic interaction. (i-p) Snapshots for velocity field $\mathbf{v} = (v_1, v_2)$ at different times. Weak flows are present due to hydrodynamic effect during the phase evolution. The nontrivial velocity leads to different phase morphology in the end compared to the case without hydrodynamic interaction.

where $h(\rho_1, \rho_2, T)$ is defined in (6.3), and the reformulated, quadratized energy formula as follows

$$\begin{aligned} E_h^n &= (q_1^n, q_1^n)_2 + \tfrac{\alpha_1}{2}(\rho_1^n, \rho_1^n)_2 + \tfrac{\alpha_2}{2}(\rho_2^n, \rho_2^n)_2 - (A, 1)_2 \\ &+ \tfrac{1}{2}\kappa_{\rho_1\rho_1}(\nabla\rho_1^n, \nabla\rho_1^n)_h + \tfrac{1}{2}\kappa_{\rho_2\rho_2}(\nabla\rho_2^n, \nabla\rho_2^n)_h + \kappa_{\rho_1\rho_2}(\nabla\rho_1^n, \nabla\rho_2^n)_h. \end{aligned} \tag{6.13}$$

Fig. 6.5-(b) depicts the total free energy of the phase separation with hydrodynamics calculated using the original formula

$$\begin{aligned} E_h^n &= \tfrac{1}{2}[u^n, u^n]_{ew} + \tfrac{1}{2}[v^n, v^n]_{ns} + (h(\rho_1^n, \rho_2^n, T), 1)_2 \\ &+ \tfrac{1}{2}\kappa_{\rho_1\rho_1}(\nabla\rho_1^n, \nabla\rho_1^n)_h + \tfrac{1}{2}\kappa_{\rho_2\rho_2}(\nabla\rho_2^n, \nabla\rho_2^n)_h + \kappa_{\rho_1\rho_2}(\nabla\rho_1^n, \nabla\rho_2^n)_h, \end{aligned} \tag{6.14}$$

where $h(\rho_1, \rho_2, T)$ is defined in (6.3), and the reformulated, quadratized energy formula as follows

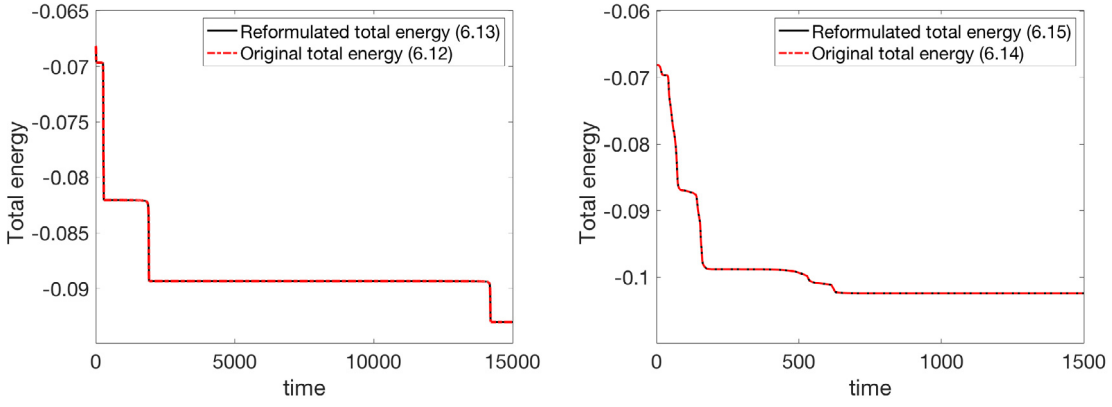

(a) Total Energy (b) Total Energy

Fig. 6.5. (a) Comparison of the total energy given by (6.12) and the one by (6.13), respectively, in phase separation processes without hydrodynamics. (b) Comparison of the total energy given by (6.14) and the one by (6.15) in phase separation processes with hydrodynamics. $\alpha_1 = \alpha_2 = 0$ is used in the simulations. The energy profiles are indistinguishable visually.

$$E_h^n = \frac{1}{2}[u^n, u^n]_{ew} + \frac{1}{2}[v^n, v^n]_{ns} + (q_1^n, q_1^n)_2 + \frac{\alpha_1}{2}(\rho_1^n, \rho_1^n)_2 + \frac{\alpha_2}{2}(\rho_2^n, \rho_2^n)_2 - (A, 1)_2$$
$$+\frac{1}{2}\kappa_{\rho_1\rho_1}(\nabla\rho_1^n, \nabla\rho_1^n)_h + \frac{1}{2}\kappa_{\rho_2\rho_2}(\nabla\rho_2^n, \nabla\rho_2^n)_h + \kappa_{\rho_1\rho_2}(\nabla\rho_1^n, \nabla\rho_2^n)_h. \tag{6.15}$$

The results are nearly indistinguishable. This attests the accuracy of the scheme developed using the EQ method.

6.3. Dynamics of gas-liquid mixtures

The compressible fluid model has many applications in the petroleum industry, where mixtures of non-hydrocarbons and hydrocarbons are abundant, such as in petroleum reservoirs or natural gas pipelines. Understanding their thermodynamic and hydrodynamic properties can help one to improve petroleum quality and yield significantly.

In the past, several equations of state had been developed to describe the relation among state variables (e.g. the volume, pressure and temperature) under a given set of physical conditions for compressible fluids. The Peng-Robinson equation of state (PR EOS) [41] is one of the popular ones, which has been successfully applied to thermodynamic and volumetric calculations in both industries and academics. Specifically, PR EOS provides reasonable accuracy near the critical point, which makes it a good choice for gas-condensate systems in the petroleum industry. For this reason, we adopt it in a hydrocarbon mixture of methane and n-decane to show the performance of our model in simulating hydrodynamics of the hydrocarbon mixtures. Many properties of mixtures can be studied by our mathematical model, such as mass adsorption of one component in the mixture on the interface between two phases near the equilibrium state, surface tension and even verification of mixing rules in the mixture. In this example, we will focus on hydrodynamics of a hydrocarbon mixture with an unstable gas-liquid interface and study the mass adsorption phenomena at the interface from the point of view of the free energy near an equilibrium state.

The free energy density function derived from PR EOS reads

$$f = f_b + h(\mathbf{n}, T), \tag{6.16}$$

where $f_b = \frac{1}{2}\sum_{i,j=1}^{N} c_{i,j}\nabla n_i \cdot \nabla n_j$ is the conformational energy with coefficients $c_{i,j}$. The bulk free energy density function $h(\mathbf{n}, T)$ is given in (2.22).

Remark 6.1. Since f^{ideal} changes rapidly near the origin which may introduce singularity in numerical simulations, we regularize this term near the origin as follows

$$f^{ideal} = \begin{cases} RTn_i(ln(\epsilon) - 1) + RT(\frac{1}{2\epsilon}n_i^2 - \frac{\epsilon}{2}), & \text{if} \quad n_i < \epsilon, \\ RTn_i(ln(n_i) - 1), & \text{otherwise,} \end{cases} \tag{6.17}$$

where $\epsilon > 0$. Corresponding to the modification, the chemical potential is changed to

$$\mu^{ideal} = \begin{cases} RT(ln(\epsilon) - 1) + RT(\frac{1}{\epsilon}n_i), & \text{if} \quad n_i < \epsilon, \\ RTln(n_i), & \text{otherwise.} \end{cases} \tag{6.18}$$

Table 6.3
Dimensional critical parameters.

Symbol	T_c (K)	P_c (MPa)	w	m (kg·mol^{-1})
n-decane ($C_{10}H_{22}$)	617.7	2.103	0.4884	0.14228
Methane (CH_4)	190.564	4.5992	0.01142	0.0160428

Table 6.4
Dimensionless critical parameters.

Symbol	T_c	P_c	w	m
n-decane ($C_{10}H_{22}$)	2.2626	1.3495	0.4884	8.8688
methane (CH_4)	0.6980	2.9513	0.01142	1

We consider a mixture of methane and n-decane in a square domain with the length of 80 nm on each side. We denote the molar density of n-decane as n_1 and that of methane as n_2, respectively. In Table 6.3, we list the dimensional parameters related to these two components. Other parameter values [12] are chosen as follows

$$\begin{aligned} &\eta_1 = \eta_2 = 1 \times 10^{-4}\ \text{Pa·s}, \quad \overline{\eta}_1 = \overline{\eta}_2 = 0.33 \times 10^{-4}\ \text{Pa·s}, \quad M_1 = 1 \times 10^{-12}\ \text{m}^2\text{·s}^{-1}, \\ &\kappa_{n_1n_1} = 1.1246 \times 10^{-18}, \quad \kappa_{n_2n_2} = 2.8649 \times 10^{-20}, \quad \kappa_{n_1n_2} = 8.9748 \times 10^{-20}. \end{aligned} \tag{6.19}$$

The gas constant is $R = 8.3144598\ \text{J·mol}^{-1}\text{·K}^{-1}$, the temperature $T = 330$ K.

The initial conditions are given by

$$n_i = \begin{cases} n_i^{liquid}, & (x^2 + y^2) \le (r_1 + r_2 \times cos(n \times arctan(\frac{x}{y})))^2 \quad \text{in } [-4 \times 10^{-8}\ \text{m},\ 4 \times 10^{-8}\ \text{m}]^2, \\ n_i^{gas}, & \text{otherwise} \quad \text{in } [-4 \times 10^{-8}\ \text{m},\ 4 \times 10^{-8}\ \text{m}]^2, \end{cases} \tag{6.20}$$

where $r_1 = 1$, $r_2 = 0.2$, $n = 8$ and

$$\begin{aligned} &n_1^{liquid} = 3814.6\ \text{mol·m}^{-3}, \quad n_1^{gas} = 26.5\ \text{mol·m}^{-3}, \\ &n_2^{liquid} = 3513.2\ \text{mol·m}^{-3}, \quad n_2^{gas} = 7133.9\ \text{mol·m}^{-3}. \end{aligned} \tag{6.21}$$

If we take characteristic molar density $n_0 = 10^3\ \text{mol·m}^{-3}$, characteristic density $\rho_0 = n_0 m_2 = 16.0428\text{kg·m}^{-3}$, characteristic length $h = 2 \times 10^{-8}$ m, characteristic time $t_0 = 6.4171 \times 10^{-11}$ s, and characteristic temperature $T_0 = 273$ K, we obtain dimensionless parameter values as follows

$$\begin{aligned} &Re_{1s} = Re_{2s} = 1, \quad Re_{1v} = Re_{2v} = 3, \quad M_1 = 9.7136 \times 10^{-4}, \\ &\kappa_{n_1n_1} = 0.0018, \quad \kappa_{n_2n_2} = 4.5961 \times 10^{-5}, \quad \kappa_{n_1n_2} = 1.4398 \times 10^{-4}. \end{aligned} \tag{6.22}$$

Other dimensionless critical parameters of the methane and n-decane are given in Table 6.4. Through the non-dimensionalization, the gas constant R results in a constant $R_0 = 1.4566$, the dimensionless temperature $T = 1.2088$. The corresponding dimensionless initial conditions become

$$n_i = \begin{cases} n_i^{liquid}, & (x^2 + y^2) \le (r_1 + r_2 \times cos(n \times arctan(\frac{x}{y})))^2 \quad \text{in } [-2, 2] \times [-2, 2], \\ n_i^{gas}, & \text{otherwise} \quad \text{in } [-2, 2] \times [-2, 2], \end{cases} \tag{6.23}$$

where $r_1 = 1$, $r_2 = 0.2$, $n = 8$ and

$$n_1^{liquid} = 3.8146, \quad n_1^{gas} = 0.0265, \quad n_2^{liquid} = 3.5132, \quad n_2^{gas} = 7.1339. \tag{6.24}$$

The governing system of equations is structurally identical to the one formulated using densities. Thus, the scheme works the same way on this model as on the one formulated using densities. Shown in Fig. 6.6, we perturb the initial condition with certain roughness on the interface, which is unstable due to the surface tension. As time elapses, the roughness vanishes, leading to a surface with the minimal surface tension on it (shown in Fig. 6.8-b). The corresponding time evolution of velocities are shown in Fig. 6.7, which demonstrates that hydrodynamics indeed speeds up evolution of the system to the steady states.

6.3.1. Density profiles and mass absorption at the interface in equilibrium

Near equilibrium ($t = 6000$), we show the density profiles of the two fluid components at $y = 0$ in Fig. 6.9-a and observe mass absorption of methane at the interface. At the equilibrium states of a phase co-existing system, two (or more) bulk phases have equivalent chemical potentials, i.e. they lie on the same tangent line (or surface) of the bulk free energy function. For most of free energy functions, such as Peng-Robinson free energy, it is not straightforward to find the

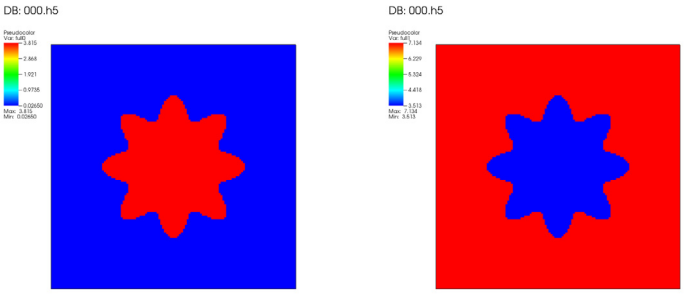

(a) Initial condition of n-decane ($C_{10}H_{22}$) (b) Initial condition of methane (CH_4)

Fig. 6.6. Initial conditions of two components in gas-liquid mixture.

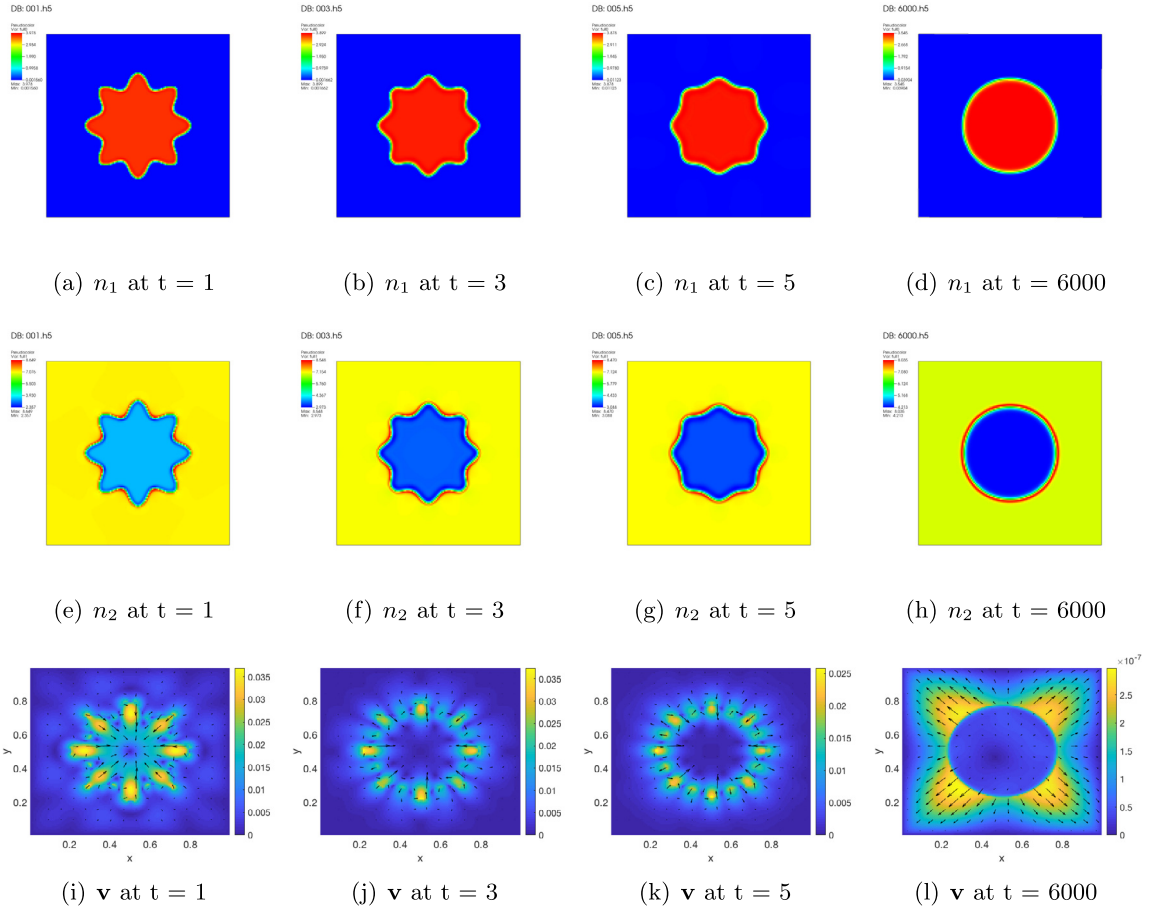

(a) n_1 at t = 1 (b) n_1 at t = 3 (c) n_1 at t = 5 (d) n_1 at t = 6000

(e) n_2 at t = 1 (f) n_2 at t = 3 (g) n_2 at t = 5 (h) n_2 at t = 6000

(i) $\mathbf{v}$ at t = 1 (j) $\mathbf{v}$ at t = 3 (k) $\mathbf{v}$ at t = 5 (l) $\mathbf{v}$ at t = 6000

Fig. 6.7. (a-d) Snapshots of n_1 at $t = 1$, 3, 5, 6000. (e-h) Snapshots of n_2. (i-l) The corresponding velocity fields.

equilibrium states by observing the graph of the free energy function directly. Following the work reported in [36,42], we subtract the tangent line (or surface) from the Helmholtz free energy density function to make the equilibrium states as the minimum points, which are easily observed, i.e. we modify the bulk free energy as follows

$$h_m(\mathbf{n}, T) = h(\mathbf{n}, T) - \sum_{i=1}^{2} \mu_i^0 n_i, \tag{6.25}$$

where $\mu_i^0, i = 1, 2$ represents the chemical potential of the ith component at the bulk equilibrium state, respectively. We show the modified free energy contour in Fig. 6.9-b. The red line is the energy path of density profiles at the equilibrium

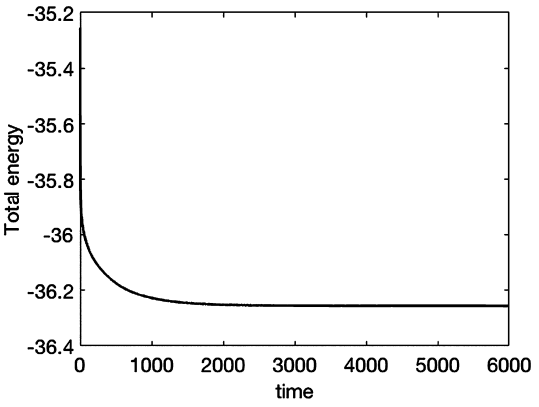

(a) Total Energy

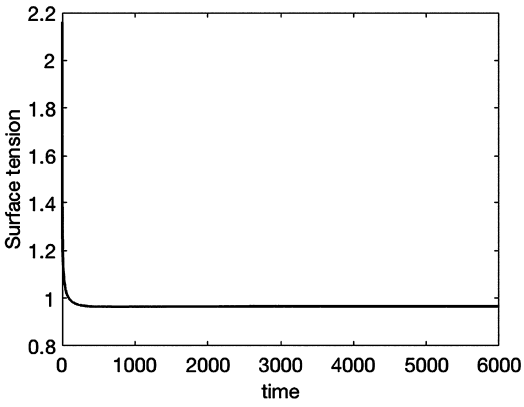

(b) Surface tension

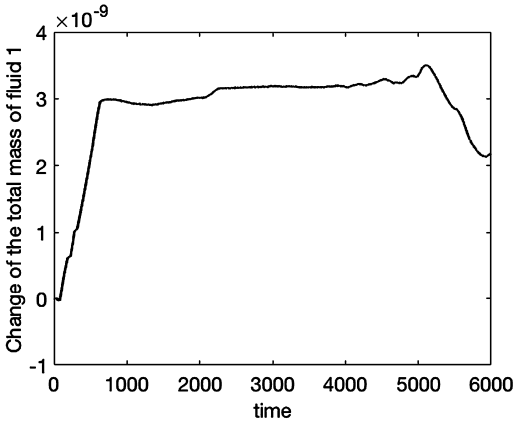

(c) The difference of total mass of the component 2 with its initial total mass

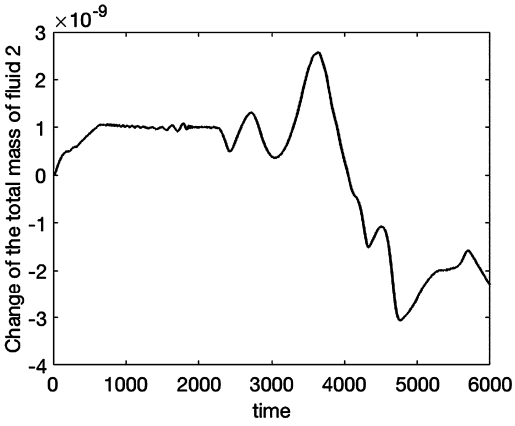

(d) The difference of total mass of the component 2 with its initial total mass

Fig. 6.8. (a) Total energy of the system (3.5) with the Peng-Robinson bulk free energy (6.16); (b) Surface tension of the mixture; (c, d) Total mass of the component 1 and 2 on the rectangular domain $\Omega = [-2, 2] \times [-2, 2]$, solved in the system (3.5) with the Peng-Robinson bulk free energy (6.16). (e) Density profiles of n-decane and methane ($y = 0$) at the equilibrium state; (f) Free energy contour. Green points represent the densities of n-decane and methane at bulk area and red circles represent their densities on the interface at equilibrium state.

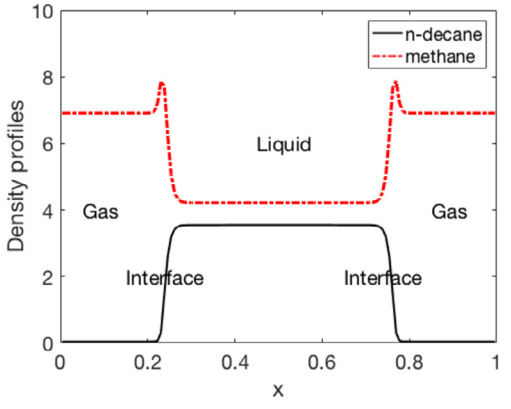

(a) Density profiles at equilibrium state (t = 6000)

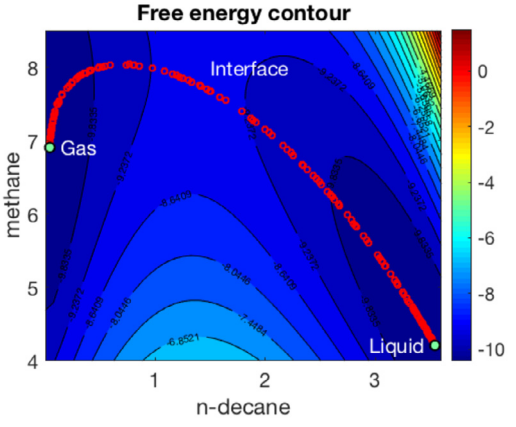

(b) Free energy contour at equilibrium state (t = 6000)

Fig. 6.9. (a) Density profiles of n-decane and methane ($y = 0$) at the equilibrium state; (b) Free energy contour. Green points represent the densities of n-decane and methane at bulk area and red circles represent their densities on the interface at equilibrium state.

state. To avoid high free energy, n-decane and methane change from one equilibrium state (Gas) to another equilibrium state (Liquid) through the saddle point of the free energy surface. Thus, the methane has a higher density on the interface than the bulk states, leading to the mass absorption phenomena on the interface.

The total energy and total mass difference with the initial condition for each component are shown in Fig. 6.8, which verifies energy stability and mass conservation of our numerical scheme.

This experiment not only shows that our mathematical model can be applied to study thermodynamic and hydrodynamic properties of the fluid mixtures in an application relevant to the petroleum industry, but also reflects that our numerical scheme can handle the Navier-Stokes-Cahn-Hilliard equation system with a highly nonlinear free energy such as the one given by (6.16).

7. Conclusion

In this paper, we have presented a second order, fully-discrete, linear and unconditionally energy stable numerical scheme for the hydrodynamic phase field model of binary compressible fluid flows. Firstly, we reformulate the model by introducing a couple of intermediate variables following the Energy Quadratization strategy. Using the reformulated model equations, we develop a second order, energy stable, semi-discrete numerical scheme in time. Then, we obtain a fully discrete numerical scheme by applying the finite difference method on the staggered grid in space, which preserves a fully discrete energy dissipation law. In addition, the solution uniqueness of the linear system resulting from the numerical scheme is proved rigorously. Several numerical experiments are presented to verify the accuracy, stability and efficiency of our numerical scheme. The comparison between the simulations with and without hydrodynamics is used to demonstrate effects of hydrodynamics in phase separation phenomena in binary compressible fluid flows. The scheme can be readily extended to models of N-component compressible fluid flows with $N > 2$.

Acknowledgements

Qi Wang's research is partially supported by NSF awards DMS-1517347, DMS-1815921, OIA-1655740 and a GEAR award from SC EPSCoR/IDeA Program.

Appendix A. Linear system resulting from the numerical scheme

For simplicity, we drop the superscript $n+1$ on the unknowns and superscript n on the right hand side terms while retaining the superscripts on the extrapolated terms. We summarize the linear system resulting from the fully discrete numerical scheme in section 5.3 as follows:

$$
\begin{cases}
\Big\{2\frac{\rho_1}{\Delta t} + d_x(A_x(\overline{\rho}_1^{n+1/2}\overline{\frac{1}{\sqrt{\rho}}}^{n+1/2})u) + d_y(A_y(\overline{\rho}_1^{n+1/2}\overline{\frac{1}{\sqrt{\rho}}}^{n+1/2})v) = \\
M_1\Delta_h\mu_1 - M_1\Delta_h\mu_2 + g_1\Big\}|_{i,j}, i = 1,\cdots,N_x, j = 1,\cdots,N_y, \\
\Big\{2\frac{\rho_2}{\Delta t} + d_x(A_x(\overline{\rho}_2^{n+1/2}\overline{\frac{1}{\sqrt{\rho}}}^{n+1/2})u) + d_y(A_y(\overline{\rho}_2^{n+1/2}\overline{\frac{1}{\sqrt{\rho}}}^{n+1/2})v) = \\
-M_1\Delta_h\mu_1 + M_1\Delta_h\mu_2 + g_2\Big\}|_{i,j}, i = 1,\cdots,N_x, j = 1,\cdots,N_y, \\
\Big\{2\frac{u}{\Delta t} + \frac{1}{2}(\overline{u}^{n+1/2}D_x(\overline{\frac{1}{\sqrt{\rho}}}^{n+1/2}a_x u) + A_x(\overline{\frac{1}{\sqrt{\rho}}}^{n+1/2}d_x(\overline{u}^{n+1/2}u))) \\
+\frac{1}{2}(a_x(A_x\overline{v}^{n+1/2}D_y(A_x(\overline{\frac{1}{\sqrt{\rho}}}^{n+1/2})u)) + A_x(\overline{\frac{1}{\sqrt{\rho}}}^{n+1/2})d_y(A_y u A_x(\overline{v}^{n+1/2})) \\
= T_1(u,v,\mu_1,\mu_2) + g_3\Big\}|_{i+\frac{1}{2},j}, i = 1,\cdots,N_x-1, j = 1,\cdots,N_y, \\
\Big\{2\frac{v}{\Delta t} + \frac{1}{2}(a_x(A_y\overline{u}^{n+1/2}D_x(A_y(\overline{\frac{1}{\sqrt{\rho}}}^{n+1/2})v)) + A_y(\overline{\frac{1}{\sqrt{\rho}}}^{n+1/2})d_x(A_y\overline{u}^{n+1/2}A_x v)) \\
+\frac{1}{2}(\overline{v}^{n+1/2}D_y(\overline{\frac{1}{\sqrt{\rho}}}^{n+1/2}a_y v) + A_y(\overline{\frac{1}{\sqrt{\rho}}}^{n+1/2}d_y(\overline{v}^{n+1/2}v))) \\
= T_2(u,v,\mu_1,\mu_2) + g_4\Big\}|_{i,j+\frac{1}{2}}, i = 1,\cdots,N_x, j = 1,\cdots,N_y-1. \\
\Big\{4\frac{q_1}{\Delta t} = 4\overline{\frac{\partial q_1}{\partial\rho_1}}^{n+1/2}\frac{\rho_1}{\Delta t} + 4\overline{\frac{\partial q_1}{\partial\rho_2}}^{n+1/2}\frac{\rho_2}{\Delta t} + g_5\Big\}|_{i,j}, i = 1,\cdots,N_x, j = 1,\cdots,N_y, \\
\Big\{-\frac{2}{\Delta t}\mu_1 = -4q_1\frac{1}{\Delta t}\overline{\frac{\partial q_1}{\partial\rho_1}}^{n+1/2} + \frac{2}{\Delta t}\kappa_{\rho_1\rho_1}\Delta_h\rho_1 + \frac{2}{\Delta t}\kappa_{\rho_1\rho_2}\Delta_h\rho_2 - \frac{2\alpha_1\rho_1}{\Delta t} + g_6\Big\}|_{i,j}, \\
i = 1,\cdots,N_x, j = 1,\cdots,N_y, \\
\Big\{-\frac{2}{\Delta t}\mu_2 = -4q_1\frac{1}{\Delta t}\overline{\frac{\partial q_1}{\partial\rho_2}}^{n+1/2} + \frac{2}{\Delta t}\kappa_{\rho_2\rho_2}\Delta_h\rho_2 + \frac{2}{\Delta t}\kappa_{\rho_1\rho_2}\Delta_h\rho_1 - \frac{2\alpha_2\rho_1}{\Delta t} + g_7\Big\}|_{i,j}, \\
i = 1,\cdots,N_x, j = 1,\cdots,N_y,
\end{cases}
\tag{A.1}
$$

where $\mu_1, \mu_2, u, v, q_1, \rho_1, \rho_2$ are the unknowns of the linear system, $g_1, g_2, g_3, g_4, g_5, g_6, g_7$ represent all the terms at the nth time steps on the right hand side. We assume that $\rho_i, \mu_i, i = 1, 2$ satisfy discrete homogeneous Neumann boundary conditions (5.8), u, v the discrete homogeneous Dirichlet boundary conditions (5.9). We define $\mathbf{D}_h$ as

$$\begin{pmatrix} d_x(A_x(\overline{\frac{1}{\sqrt{\rho}}}^{n+1/2})u)) & \frac{1}{2}S \\ \frac{1}{2}S & d_y(A_y(\overline{\frac{1}{\sqrt{\rho}}}^{n+1/2})v)) \end{pmatrix}, \tag{A.2}$$

where $S = D_x(A_y(\overline{\frac{1}{\sqrt{\rho}}}^{n+1/2})v) + D_y(A_x(\overline{\frac{1}{\sqrt{\rho}}}^{n+1/2})u))$. We denote $T_1(u, v, \mu_1, \mu_2)$ and $T_2(u, v, \mu_1, \mu_2)$ as the functions of u, v, μ_1 and μ_2 as follows:

$$\begin{aligned} T_1(u, v, \mu_1, \mu_2) &= A_x(\overline{\frac{1}{\sqrt{\rho}}}^{n+1/2})(D_x(\frac{1}{Re_s}d_x(A_x(\overline{\frac{1}{\sqrt{\rho}}}^{n+1/2})u)) \\ &+d_y(A_x(A_y\frac{1}{Re_s})D_y(A_x(\overline{\frac{1}{\sqrt{\rho}}}^{n+1/2})u))) \\ &+A_x(\overline{\frac{1}{\sqrt{\rho}}}^{n+1/2})D_x(\frac{1}{Re_s}d_x(A_x(\overline{\frac{1}{\sqrt{\rho}}}^{n+1/2})u)) \\ &+A_x(\overline{\frac{1}{\sqrt{\rho}}}^{n+1/2})d_y(A_x(A_y\frac{1}{Re_s})D_x(A_y(\overline{\frac{1}{\sqrt{\rho}}}^{n+1/2})v)) \\ &+A_x(\overline{\frac{1}{\sqrt{\rho}}}^{n+1/2})D_x(\frac{1}{Re_v}d_x(A_x(\overline{\frac{1}{\sqrt{\rho}}}^{n+1/2})u)) + A_x(\overline{\frac{1}{\sqrt{\rho}}}^{n+1/2})D_x(\frac{1}{Re_v}d_y(A_y(\overline{\frac{1}{\sqrt{\rho}}}^{n+1/2})v)) \\ &-A_x(\overline{\rho_1}^{n+1/2}\overline{\frac{1}{\sqrt{\rho}}}^{n+1/2})D_x(\mu_1) - A_x(\overline{\rho_2}^{n+1/2}\overline{\frac{1}{\sqrt{\rho}}}^{n+1/2})D_x(\mu_2), \end{aligned} \tag{A.3}$$

$$\begin{aligned} T_2(u, v, \mu_1, \mu_2) &= A_y(\overline{\frac{1}{\sqrt{\rho}}}^{n+1/2})(d_x(A_x(A_y\frac{1}{Re_s})D_x(A_y(\overline{\frac{1}{\sqrt{\rho}}}^{n+1/2})v)) \\ &+D_y(\frac{1}{Re_s}d_y(A_y(\overline{\frac{1}{\sqrt{\rho}}}^{n+1/2})v))) \\ &+A_y(\overline{\frac{1}{\sqrt{\rho}}}^{n+1/2})d_x(A_x(A_y\frac{1}{Re_s})D_y(A_x(\overline{\frac{1}{\sqrt{\rho}}}^{n+1/2})u)) \\ &+A_y(\overline{\frac{1}{\sqrt{\rho}}}^{n+1/2})D_y(\frac{1}{Re_s}d_y(A_y(\overline{\frac{1}{\sqrt{\rho}}}^{n+1/2})v)) \\ &+A_y(\overline{\frac{1}{\sqrt{\rho}}}^{n+1/2})D_y(\frac{1}{Re_v}d_x(A_x(\overline{\frac{1}{\sqrt{\rho}}}^{n+1/2})u)) + A_y(\overline{\frac{1}{\sqrt{\rho}}}^{n+1/2})D_y(\frac{1}{Re_v}d_y(A_y(\overline{\frac{1}{\sqrt{\rho}}}^{n+1/2})v)) \\ &-A_y(\overline{\rho_1}^{n+1/2}\overline{\frac{1}{\sqrt{\rho}}}^{n+1/2})D_y(\mu_1) - A_y(\overline{\rho_2}^{n+1/2}\overline{\frac{1}{\sqrt{\rho}}}^{n+1/2})D_y(\mu_2). \end{aligned} \tag{A.4}$$

We then rewrite system (A.9) as follows

$$\mathcal{A}\cdot\mathbf{X} = \mathcal{G}, \tag{A.5}$$

where $\mathbf{X} = (\mu_1, \mu_2, u, v, q_1, \rho_1, \rho_2)$ and $\mathcal{G} = (g_1, g_2, g_3, g_4, g_5, g_6, g_7)^T$. The coefficient matrix $\mathcal{A}$ is given as follows

$$\begin{pmatrix} -M_1\Delta_h(\cdot) & M_1\Delta_h(\cdot) & A_{1u} & A_{1v} & 0 & 2\frac{(\cdot)}{\Delta t} & 0 \\ M_1\Delta_h(\cdot) & -M_1\Delta_h(\cdot) & A_{2u} & A_{2v} & 0 & 0 & 2\frac{(\cdot)}{\Delta t} \\ -T_{1\mu_1} & -T_{1\mu_2} & A_{3u} & -T_{1v} & 0 & 0 & 0 \\ -T_{2\mu_1} & -T_{2\mu_2} & -T_{2u} & A_{4v} & 0 & 0 & 0 \\ 0 & 0 & 0 & 0 & 4\frac{(\cdot)}{\Delta t} & -4\overline{\frac{\partial q_1}{\partial\rho_1}}^{n+1/2}\frac{(\cdot)}{\Delta t} & -4\overline{\frac{\partial q_1}{\partial\rho_2}}^{n+1/2}\frac{(\cdot)}{\Delta t} \\ -\frac{2}{\Delta t}(\cdot) & 0 & 0 & 0 & 4\frac{1}{\Delta t}\overline{\frac{\partial q_1}{\partial\rho_1}}^{n+1/2}(\cdot) & -\frac{2\kappa_{\rho_1\rho_1}}{\Delta t}\Delta_h(\cdot) + \frac{2\alpha_1}{\Delta t} & -\frac{2\kappa_{\rho_1\rho_2}}{\Delta t}\Delta_h(\cdot) \\ 0 & -\frac{2}{\Delta t}(\cdot) & 0 & 0 & 4\frac{1}{\Delta t}\overline{\frac{\partial q_1}{\partial\rho_2}}^{n+1/2}(\cdot) & -\frac{2\kappa_{\rho_1\rho_2}}{\Delta t}\Delta_h(\cdot) & -\frac{2\kappa_{\rho_2\rho_2}}{\Delta t}\Delta_h(\cdot) + \frac{2\alpha_2}{\Delta t} \end{pmatrix}, \tag{A.6}$$

where

$$
\begin{aligned}
&A_{1u} = d_x(A_x(\overline{\rho}_1^{n+1/2}\overline{\frac{1}{\sqrt{\rho}}}^{n+1/2})(\cdot)), \qquad A_{1v} = d_y(A_y(\overline{\rho}_1^{n+1/2}\overline{\frac{1}{\sqrt{\rho}}}^{n+1/2})(\cdot)),\\
&A_{2u} = d_x(A_x(\overline{\rho}_2^{n+1/2}\overline{\frac{1}{\sqrt{\rho}}}^{n+1/2})(\cdot)), \qquad A_{2v} = d_y(A_y(\overline{\rho}_2^{n+1/2}\overline{\frac{1}{\sqrt{\rho}}}^{n+1/2})(\cdot)),\\
&A_{3u} = 2\tfrac{(\cdot)}{\Delta t} + \tfrac{1}{2}(\overline{u}^{n+1/2}D_x(\overline{\frac{1}{\sqrt{\rho}}}^{n+1/2}a_x(\cdot)) + A_x(\overline{\frac{1}{\sqrt{\rho}}}^{n+1/2}d_x(\overline{u}^{n+1/2}(\cdot))))\\
&+\tfrac{1}{2}(a_x(A_x\overline{v}^{n+1/2}D_y(A_x(\overline{\frac{1}{\sqrt{\rho}}}^{n+1/2})(\cdot))) + A_x(\overline{\frac{1}{\sqrt{\rho}}}^{n+1/2})d_y(A_y(\cdot)A_x(\overline{v}^{n+1/2})) - T_{1u},\\
&A_{4v} = 2\tfrac{(\cdot)}{\Delta t} + \tfrac{1}{2}(a_x(A_y{}^{n+1/2}D_x(A_y(\overline{\frac{1}{\sqrt{\rho}}}^{n+1/2})(\cdot)))\\
&+A_y(\overline{\frac{1}{\sqrt{\rho}}}^{n+1/2})d_x(A_y\overline{u}^{n+1/2}A_x(\cdot)))\\
&+\tfrac{1}{2}(\overline{v}^{n+1/2}D_y(\overline{\frac{1}{\sqrt{\rho}}}^{n+1/2}a_y(\cdot)) + A_y(\overline{\frac{1}{\sqrt{\rho}}}^{n+1/2}d_y(\overline{v}^{n+1/2}(\cdot)))) - T_{2v},\\
&T_{1u} = A_x(\overline{\frac{1}{\sqrt{\rho}}}^{n+1/2})(D_x(\tfrac{1}{Re_s}d_x(A_x(\overline{\frac{1}{\sqrt{\rho}}}^{n+1/2})(\cdot)))\\
&+d_y(A_x(A_y\tfrac{1}{Re_s})D_y(A_x(\overline{\frac{1}{\sqrt{\rho}}}^{n+1/2})(\cdot))))\\
&+A_x(\overline{\frac{1}{\sqrt{\rho}}}^{n+1/2})D_x(\tfrac{1}{Re_s}d_x(A_x(\overline{\frac{1}{\sqrt{\rho}}}^{n+1/2})(\cdot)))\\
&+A_x(\overline{\frac{1}{\sqrt{\rho}}}^{n+1/2})D_x(\tfrac{1}{Re_v}d_x(A_x(\overline{\frac{1}{\sqrt{\rho}}}^{n+1/2})(\cdot))),\\
&T_{1v} = +A_x(\overline{\frac{1}{\sqrt{\rho}}}^{n+1/2})d_y(A_x(A_y\tfrac{1}{Re_s})D_x(A_y(\overline{\frac{1}{\sqrt{\rho}}}^{n+1/2})(\cdot)))\\
&+A_x(\overline{\frac{1}{\sqrt{\rho}}}^{n+1/2})D_x(\tfrac{1}{Re_v}d_y(A_y(\overline{\frac{1}{\sqrt{\rho}}}^{n+1/2})(\cdot))),\\
&T_{1\mu_1} = -A_x(\overline{\rho_1}^{n+1/2}\overline{\frac{1}{\sqrt{\rho}}}^{n+1/2})D_x(\cdot), \qquad T_{2\mu_2} = -A_x(\overline{\rho_2}^{n+1/2}\overline{\frac{1}{\sqrt{\rho}}}^{n+1/2})D_x(\cdot),\\
&T_{2v} = A_y(\overline{\frac{1}{\sqrt{\rho}}}^{n+1/2})(d_x(A_x(A_y\tfrac{1}{Re_s})D_x(A_y(\overline{\frac{1}{\sqrt{\rho}}}^{n+1/2})(\cdot))) + D_y(\tfrac{1}{Re_s}d_y(A_y(\overline{\frac{1}{\sqrt{\rho}}}^{n+1/2})(\cdot))))\\
&+A_y(\overline{\frac{1}{\sqrt{\rho}}}^{n+1/2})D_y(\tfrac{1}{Re_s}d_y(A_y(\overline{\frac{1}{\sqrt{\rho}}}^{n+1/2})(\cdot))) + A_y(\overline{\frac{1}{\sqrt{\rho}}}^{n+1/2})D_y(\tfrac{1}{Re_v}d_y(A_y(\overline{\frac{1}{\sqrt{\rho}}}^{n+1/2})(\cdot))),\\
&T_{2u} = +A_y(\overline{\frac{1}{\sqrt{\rho}}}^{n+1/2})d_x(A_x(A_y\tfrac{1}{Re_s})D_y(A_x(\overline{\frac{1}{\sqrt{\rho}}}^{n+1/2})(\cdot)))\\
&+A_y(\overline{\frac{1}{\sqrt{\rho}}}^{n+1/2})D_y(\tfrac{1}{Re_v}d_x(A_x(\overline{\frac{1}{\sqrt{\rho}}}^{n+1/2})(\cdot))),\\
&T_{2\mu_1} = -A_y(\overline{\rho_1}^{n+1/2}\overline{\frac{1}{\sqrt{\rho}}}^{n+1/2})D_y(\cdot), \qquad T_{2\mu_2} = -A_y(\overline{\rho_2}^{n+1/2}\overline{\frac{1}{\sqrt{\rho}}}^{n+1/2})D_y(\cdot).
\end{aligned}
\tag{A.7}
$$

$$
\tag{A.8}
$$

The corresponding homogeneous system is given by

$$
\mathcal{A}\cdot\mathbf{X} = 0. \tag{A.9}
$$

Appendix B. Supplementary material

Supplementary material related to this article can be found online at https://doi.org/10.1016/j.jcp.2019.06.030.

References

[1] Helmut Abels, On a diffuse interface model for two-phase flows of viscous, incompressible fluids with matched densities, Arch. Ration. Mech. Anal. 194 (2) (Nov 2009) 463–506.

[2] S. Aland, S. Egerer, J. Lowengrub, A. Voigt, Diffuse interface models of locally inextensible vesicles in a viscous fluid, J. Comput. Phys. 277 (2014) 32–47.

[3] S. Aland, J. Lowengrub, A. Voigt, Particles at fluid-fluid interfaces: a new Navier-Stokes-Cahn-Hilliard surface-phase-field model, Phys. Rev. E 86 (4) (2012).

[4] A. Bertozzi, S. Esedoglu, A. Gillette, Inpainting of binary images using the Cahn-Hilliard equation, IEEE Trans. Image Process. 16 (1) (2007) 285–291.

[5] M. Borden, C. Verhoosej, M. Scott, T. Hughes, C. Landis, A phase-field description of dynamic brittle fracture, Comput. Methods Appl. Mech. Eng. 217 (220) (2012) 77–95.
[6] B. Camley, Y. Zhao, Bo Li, H. Levine, W. Rappel, Crawling and turning in a minimal reaction-diffusion cell motility model: coupling cell shape and biochemistry, Phys. Rev. E 95 (012401) (2017).
[7] L.Q. Chen, W. Yang, Computer simulation of the dynamics of a quenched system with large number of non-conserved order parameters, Phys. Rev. B 60 (1994) 15752–15756.
[8] Wenbin Chen, Wenqiang Feng, Yuan Liu, Cheng Wang, Steven M. Wise, A second order energy stable scheme for the Cahn-Hilliard-Hele-Shaw equations, Discrete Contin. Dyn. Syst., Ser. B 22 (1) (2018).
[9] Y. Chen, J. Shen, Efficient adaptive energy stable schemes for the incompressible Cahn-Hilliard Navier-Stokes phase-field models, J. Comput. Phys. 308 (2016) 40–56.
[10] Kelong Cheng, Wenqiang Feng, Cheng Wang, Steven M. Wise, An energy stable fourth order finite difference scheme for the Cahn-Hilliard equation, J. Comput. Appl. Math. (2018).
[11] C. Collins, J. Shen, S.M. Wise, An efficient, energy stable scheme for the Cahn-Hilliard-Brinkman system, Commun. Comput. Phys. 13 (04) (2013) 929–957.
[12] Alvin S. Cullick, Melwyn L. Mathis, Densities and viscosities of mixtures of carbon dioxide and n-decane from 310 to 403 K and 7 to 30 Mpa, J. Chem. Eng. Data 29 (4) (1984) 393–396.
[13] M. Doi, S.F. Edwards, The Theory of Polymer Dynamics, Oxford Science Publication, 1986.
[14] Q. Du, C. Liu, R. Ryham, X. Wang, A phase field formulation of the Willmore problem, Nonlinearity 18 (2005) 1249–1267.
[15] C.M. Elliott, A.M. Stuart, The global dynamics of discrete semilinear parabolic equations, SIAM J. Numer. Anal. 30 (1993) 1622–1663.
[16] D. Eyre, Unconditionally gradient stable time marching the Cahn-Hilliard equation, in: Computational and Mathematical Models of Microstructural Evolution, San Francisco, CA, 1998, vol. 529, 1998, pp. 39–46.
[17] P.J. Flory, Principles of Polymer Chemistry, Cornell University Press, 1953.
[18] Nir Gavish, Gurgen Hayrapetyan, Keith Promislow, Li Yang, Curvature driven flow of bilayer interfaces, Physica D 240 (2011) 675–693.
[19] Yuezheng Gong, Jia Zhao, Qi Wang, An energy stable algorithm for a quasi-incompressible hydrodynamic phase-field model of viscous fluid mixtures with variable densities and viscosities, Comput. Phys. Commun. 219 (2017) 20–34.
[20] Yuezheng Gong, Jia Zhao, Qi Wang, Second order fully discrete energy stable methods on staggered grids for hydrodynamic phase field models of binary viscous fluids, SIAM J. Sci. Comput. 40 (2) (2018) B528–B553.
[21] Yuezheng Gong, Jia Zhao, Xiaogang Yang, Qi Wang, Fully discrete second-order linear schemes for hydrodynamic phase field models of binary viscous fluid flows with variable densities, SIAM J. Sci. Comput. 40 (1) (2018) B138–B167.
[22] F. Guillén-González, G. Tierra, On linear schemes for a Cahn-Hilliard diffuse interface model, J. Comput. Phys. 234 (2013) 140–171.
[23] Z. Guo, P. Lin, J. Lowengrub, S. Wise, Mass conservative and energy stable finite difference methods for the quasi-incompressible Navier-Stokes-Cahn-Hilliard system: primitive variable and projection-type schemes, Comput. Methods Appl. Mech. Eng. 326 (2017) 144–174, https://doi.org/10.1016/j.cma.2017.08.011.
[24] Zhenlin Guo, Ping Lin, A thermodynamically consistent phase-field model for two-phase flows with thermocapillary effects, J. Fluid Mech. 766 (2015) 226–271.
[25] Edouard Hannezo, Alice Coucke, Jean-François Joanny, Interplay of migratory and division forces as a generic mechanism for stem cell patterns, Phys. Rev. E 93 (Feb 2016) 022405.
[26] P.C. Hohenberg, B.I. Halperin, Theory of dynamic critical phenomena, Rev. Mod. Phys. 49 (3) (1977) 435–479.
[27] Maryna Kapustina, Denis Tsygankov, Jia Zhao, Timothy Wessler, Xiaofeng Yang, Alex Chen, Nathan Roach, Timothy C. Elston, Qi Wang, Ken Jacobson, M. Gregory Forest, Modeling the excess cell surface stored in a complex morphology of bleb-like protrusions, PLoS Comput. Biol. 12 (3) (2016) 1–25, 03.
[28] Jisheng Kou, Shuyu Sun, Thermodynamically consistent modeling and simulation of multi-component two-phase flow model with partial miscibility, Comput. Methods Appl. Mech. Eng. 331 (2018) 623–649.
[29] Jisheng Kou, Shuyu Sun, Xiuhua Wang, Linearly decoupled energy-stable numerical methods for multi-component two-phase compressible flow, SIAM J. Numer. Anal. 56 (6) (2017) 3219–3248.
[30] Y. Li, J. Kim, Multiphase image segmentation using a phase-field model, Comput. Math. Appl. 62 (2011) 737–745.
[31] Hong Lin, Yuan-Yuan Duan, Surface tension measurements of propane (R-290) and isobutane (R-600a) from (253 to 333) K, J. Chem. Eng. Data 48 (5) (2003) 1360–1363.
[32] C. Liu, J. Shen, A phase field model for the mixture of two incompressible fluids and its approximation by a Fourier-spectral method, Physica D 179 (3) (2003) 211–228.
[33] J. Lober, F. Ziebert, I.S. Aranson, Modeling crawling cell movement on soft engineered substrates, Soft Matter 10 (2014) 1365.
[34] J. Lowengrub, A. Ratz, A. Voigt, Phase field modeling of the dynamics of multicomponent vesicles spinodal decomposition coarsening budding and fission, Phys. Rev. E 79 (3) (2009).
[35] J.S. Lowengrub, L. Truskinovsky, Quasi incompressible Cahn-Hilliard fluids and topological transitions, Proc. R. Soc. A 454 (1998) 2617–2654.
[36] Xiaoqun Mu, Florian Frank, Faruk O. Alpak, Walter G. Chapman, Stabilized density gradient theory algorithm for modeling interfacial properties of pure and mixed systems, Fluid Phase Equilib. 435 (2017) 118–130.
[37] S. Najem, M. Grant, Coupling actin dynamics to phase-field in modeling neural growth, Soft Matter 11 (2015) 4476.
[38] S. Najem, M. Grant, Phase-field model for collective cell migration, Phys. Rev. E 93 (052405) (2016).
[39] M. Nonomura, Study on multicellular systems using a phase field model, PLoS ONE 7 (4) (2012) 0033501.
[40] Hossein Nourozieh, Bita Bayestehparvin, Mohammad Kariznovi, Jalal Abedi, Equilibrium properties of (carbon dioxide + n-decane + n-octadecane) systems: experiments and thermodynamic modeling, J. Chem. Eng. Data 58 (5) (2013) 1236–1243.
[41] Ding-Yu Peng, Donald B. Robinson, A new two-constant equation of state, Ind. Eng. Chem. Fundam. 15 (1) (1976) 59–64.
[42] J.S. Rowlinson, B. Widom, Molecular Theory of Capillarity, Clarendon Press, Oxford, 1989.
[43] D. Shao, H. Levine, W. Pappel, Coupling actin flow, adhesion, and morphology in a computational cell motility model, Proc. Natl. Acad. Sci. USA 109 (18) (May 2012) 6855.
[44] D. Shao, W. Pappel, H. Levine, Computational model for cell morphodynamics, Phys. Rev. Lett. 105 (September 2010).
[45] J. Shen, C. Wang, X. Wang, S.M. Wise, Second-order convex splitting schemes for gradient flows with Ehrlichâ-Schwoebel type energy: application to thin film epitaxy, SIAM J. Numer. Anal. 50 (1) (2012) 105–125.
[46] J. Shen, X. Yang, Numerical approximations of Allen-Cahn and Cahn-Hilliard equations, Discrete Contin. Dyn. Syst., Ser. A 28 (2010) 1669–1691.
[47] Jie Shen, Jie Xu, Jiang Yang, The scalar auxiliary variable (SAV) approach for gradient flows, J. Comput. Phys. 353 (2018) 407–416.
[48] S. Torabi, J. Lowengrub, A. Voigt, S. Wise, A new phase-field model for strongly anisotropic systems, Proc. R. Soc. A 265 (2009) 1337–1359.
[49] X. Wang, Q. Du, Modeling and simulations of multi-component lipid membranes and open membranes via diffuse interface approaches, J. Math. Biol. 56 (2008) 347–371.
[50] S. Wise, J. Kim, J. Lowengrub, Solving the regularized strongly anisotropic Cahn-Hilliard equation by an adaptive nonlinear multigrid method, J. Comput. Phys. 226 (1) (2007) 414–446.

[51] S. Wise, J. Lowengrub, H. Frieboes, B. Cristini, Three dimensional multispecies nonlinear tumor growth I: model and numerical method, J. Theor. Biol. 253 (3) (2008) 524–543.
[52] T. Witkowski, R. Backofen, A. Voigt, The influence of membrane bound proteins on phase separation and coarsening in cell membranes, Phys. Chem. Chem. Phys. 14 (42) (2012) 14403–14712.
[53] X. Yang, Linear first and second order and unconditionally energy stable numerical schemes for the phase field model of homopolymer blends, J. Comput. Phys. 327 (2016) 294–316.
[54] X. Yang, Numerical approximations to the stochastic Cahn–Hilliard phase field model, Comput. Methods Appl. Mech. Eng. (2016), submitted for publication.
[55] X. Yang, J. Li, G. Forest, Q. Wang, Hydrodynamic theories for flows of active liquid crystals and the generalized Onsager principle, Entropy 18 (6) (2016) 202.
[56] J. Zhao, P. Seeluangsawat, Q. Wang, Modeling antimicrobial tolerance and treatment of heterogeneous biofilms, Math. Biosci. 282 (2016) 1–15.
[57] J. Zhao, Y. Shen, M. Happasalo, Z.J. Wang, Q. Wang, A 3d numerical study of antimicrobial persistence in heterogeneous multi-species biofilms, J. Theor. Biol. 392 (2016) 83–98.
[58] J. Zhao, Q. Wang, Three-dimensional numerical simulations of biofilm dynamics with quorum sensing in a flow cell, Bull. Math. Biol. 79 (4) (2017) 884–919.
[59] J. Zhao, X. Yang, Y. Gong, Q. Wang, A novel linear second order unconditionally energy-stable scheme for a hydrodynamic Q-tensor model for liquid crystals, Comput. Methods Appl. Mech. Eng. 318 (2017) 803–825.
[60] J. Li, J. Zhao, Q. Wang, Structure preserving numerical approximations of thermodynamically consistent crystal growth models, J. Comput. Phys. 382 (2019) 202–220.
[61] Jia Zhao, Qi Wang, Modeling cytokinesis of eukaryotic cells driven by the actomyosin contractile ring, Int. J. Numer. Methods Biomed. Eng. 32 (12) (2016).
[62] Jia Zhao, Xiaofeng Yang, Yuezheng Gong, Xueping Zhao, Xiaogang Yang, Jun Li, Qi Wang, A general strategy for numerical approximations of non-equilibrium models—Part I: thermodynamical systems, Int. J. Numer. Anal. Model. 15 (6) (2018) 884–918.
[63] Jia Zhao, Xiaofeng Yang, Jun Li, Qi Wang, Energy stable numerical schemes for a hydrodynamic model of nematic liquid crystals, SIAM J. Sci. Comput. 38 (2016) A3264–A3290.
[64] Xueping Zhao, Tiezheng Qian, Qi Wang, Thermodynamically consistent phase field models of multi-component compressible fluid flows, arXiv preprint, arXiv:1809.05494, 2018.
[65] L. Zhornitskaya, A. Bertozzi, Positivity-preserving numerical schemes for lubrication-type equations, SIAM J. Numer. Anal. 37 (2) (2000) 523–555.
[66] Jingzhi Zhu, Longqing Chen, Jie Shen, Veena Tikare, Coarsening kinetics from a variable-mobility Cahn-Hilliard equation: application of a semi-impliciit Fourier spectral method, Phys. Rev. E 60 (1999) 3564.
[67] F. Ziebert, I.S. Aranson, Effects of adhesion dynamics and substrate compliance on the shape and motility of crawling cells, PLoS ONE 8 (5) (2013) e64511.
[68] F. Ziebert, S. Swaminathan, I.S. Aranson, Model for self-polarization and motility of keratocyte fragments, J. R. Soc. Interface 9 (2012) 1084–1092.
[69] D. Zwicker, R. Seyboldt, C. Weber, A. Hyman, F. Julicher, Growth and division of active droplets provides a model for protocells, Nat. Phys. 13 (2017) 408–413.